ROCK-AROUND ORBITS

A Thesis

by

SCOTT KENNETH BOURGEOIS

Submitted to the Office of Graduate Studies of
Texas A&M University
in partial fulfillment of the requirements for the degree of

MASTER OF SCIENCE

December 2009

Major Subject: Aerospace Engineering

ROCK-AROUND ORBITS

A Thesis

by

SCOTT KENNETH BOURGEOIS

Submitted to the Office of Graduate Studies of
Texas A&M University
in partial fulfillment of the requirements for the degree of

MASTER OF SCIENCE

Approved by:

Chair of Committee,	Daniele Mortari
Committee Members,	David Hyland
	Tom Pollock
	J. Maurice Rojas
Head of Department,	Dimitris Lagoudas

December 2009

Major Subject: Aerospace Engineering

ABSTRACT

Rock-Around Orbits. (December 2009)
Scott Kenneth Bourgeois, B.S., Texas A&M University
Chair of Advisory Committee: Dr. Daniele Mortari

The ability to observe resident space objects (RSOs) is a necessary requirement for space situational awareness. While objects in a Low-Earth Orbit are easily observable by ground-based sensors, difficulties arise when trying to monitor objects with larger orbits far above the Earth's surface, e.g. a Geostationary Orbit. Camera systems mounted on satellites can provide an effective way to observe these objects. Using a satellite with a specific orbit relative to the RSO's orbit, one can passively observe all the objects that share the RSO's orbit over a given time without active maneuvering.

An orbit can be defined by five parameters: semi-major axis, eccentricity, right ascension of ascending node, inclination, and argument of perigee $(a, e, \Omega, i, \omega)$. Using these parameters, one can create an orbit that will surround the target orbit allowing the satellite in the Rock-Around Orbit (RAO) orbit to have a 360 degree view of RSOs in the target orbit. The RAO orbit can be applied to any circular or elliptical target orbit; and for any target orbit, there are many possible RAO orbits. Therefore, different methods are required to narrow down the selection of RAO orbits. These methods use distance limitations, time requirements, orbit perturbations, and other factors to limit the orbit selections.

The first step is to determine the range of RAO semi-major axes for any given target orbit by ensuring the RAO orbit does not exceed a prescribed maximum allowable distance, $d_{\max}$ from the target orbit. It is then necessary to determine the eccentricity range for each possible RAO semi-major axis. This is done by ensuring

the RAO still does not exceed $d_{\max}$ but also ensuring that the RAO orbit travels inside and outside of the target orbit. This comprises one half of the rock-around motion. The final step is to determine the inclination of the RAO orbit. Only a small inclination difference from that of the target orbit is required to complete the rock-around motion while the maximum inclination is found by making sure the RAO orbit does not exceed $d_{\max}$.

It is then important to consider orbit perturbations, since they can destroy the synchronization between the RAO and target orbit. By examining the effects of the linear J_2 perturbations on the right ascension of ascending node and argument of perigee, the correct semi-major axis, eccentricity, and inclination can be chosen to minimize the amount of fuel required for station keeping. The optimal values can be found by finding the Δv needed for different combinations of the variables and then choosing the values that provide the minimum Δv.

For any target orbit, there are multiple RAO orbit possibilities that can provide 360 degree coverage of a target orbit. Even after eliminating some of them based on the methods already described, there are still many possibilities. The rest of the elimination process would then be based on the mission requirements which could be the range of an on-board sensor, the thruster or reaction wheel controls, or any other number of possibilities.

To Lauren, my confessor

ACKNOWLEDGMENTS

First and foremost, I would like to thank my advisor Dr. Mortari. He gave me a research topic in which I was very interested, and then let me make it my own. He has taught me to be a better engineer and to persist because there is always an answer. I would also like to thank the staff at the Spacecraft Technology Center for their help and support. I have learned that patience is not only a good virtue to have as a person, but as an engineer too.

I could not have done this without the support of my parents, Ken and Trudy. They helped me financially and have allowed me to leave school without any debt for which I will always be grateful, but most importantly they supported me emotionally and always encouraged me to pursue my dream. Last, but certainly not least, I would like to thank my wife, Lauren, without whom this would have been a much more difficult journey. She has supported me in every way and has laid down the foundation for our future and our family.

TABLE OF CONTENTS

LIST OF TABLES

LIST OF FIGURES

FIGURE Page

FIGURE Page

FIGURE Page

CHAPTER I

INTRODUCTION

A. Flower Constellations

The theory of Flower Constellations [1, 2, 3, 4], developed at Texas A&M University, has generated many by-products [5, 6, 7] and potential solutions for Earth and space observing systems. In particular, the ability to obtain or design symmetric periodic solutions makes the theory of Flower Constellations an attractive tool to design either Earth reconnaissance systems or space surveillance systems. While Earth reconnaissance missions require the synchronization be relative to the Earth's angular velocity, space surveillance missions of certain orbits (e.g. GEO belt, LEO, multi-stationary orbits, etc.) require the synchronization be relative to the orbital period of the target orbit.

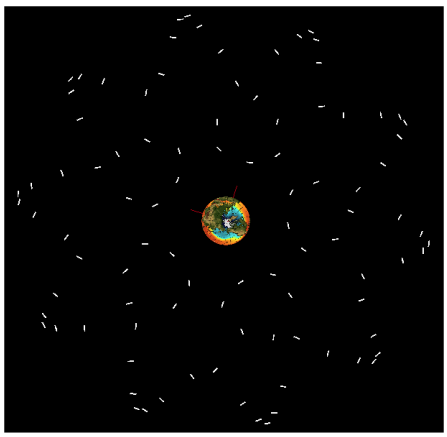

Fig. 1. Example of a Flower Constellation [1]

This thesis follows the style of *The Journal of the Astronautical Sciences*.

The theory of Flower Constellations (of which an example can be seen in Figure 1) is a unique theory of satellite constellations generally characterized by repeatable ground tracks and a suitable phasing mechanism. They are governed by two sets of values. The first are three independent integers: N_p, N_d, and N_s which are the number of petals, number of days to repeat the ground track, and the number of satellites in the constellation, respectively. The other values are the orbital parameters of the satellites - a, e, Ω, i, ω, M - which are the orbit's semi-major axis, eccentricity, right ascension of ascending node, inclination, argument of perigee, and mean anomaly, respectively. These parameters can be seen in Figures 2 and 3. To choose values for some of these parameters, the FC theory uses compatible orbits [1]. A compatible orbit can be defined as an orbit which has a period whose ratio with respect to a rotating reference frame is a rational number. Using the Earth rotating frame, this creates repeating ground tracks. The number of petals defines how many orbits are performed during the number of days needed to repeat the ground track. From this, there are an infinite number of possible Flower Constellations; however, these can be narrowed down based on the type of mission for which they are to be used.

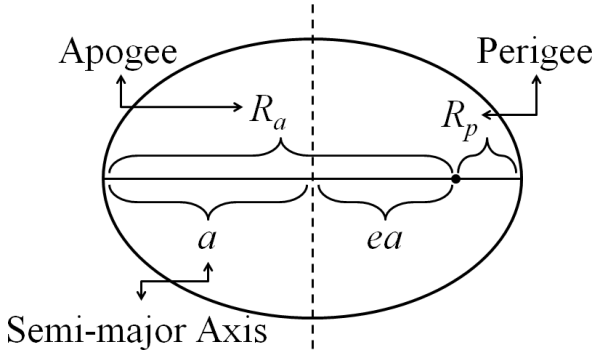

Fig. 2. Orbit Shape

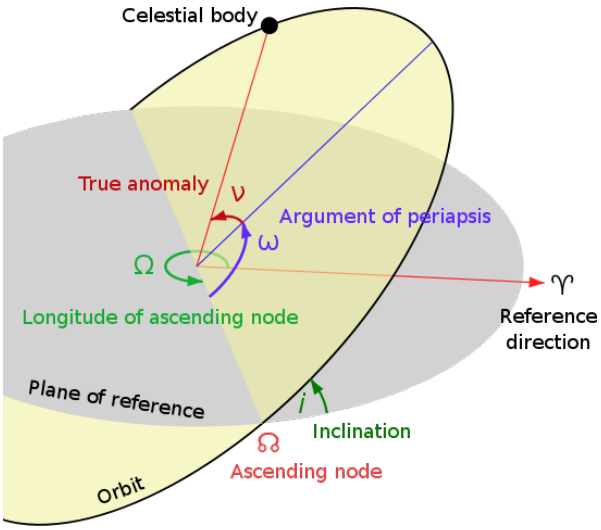

Fig. 3. Orbit Orientation [8]

B. Rock-Around Orbits

Using this theory and applying it to space observation rather than Earth observation leads to the theory of Rock-Around Orbits (RAO). The basic theory is the same except now one wants to observe a group of RSOs rather than the Earth. Therefore, the new rotating frame is based on the period of the RSOs in the same orbit or belt. Redefining the integers, we can get N_t, N_r, and $N_{d\max}$ which are the number of target orbit periods, the number of RAO periods, and the maximum number of days to complete one observation of the target orbit, respectively. This will then produce a finite number of possibilities for the period of the RAO orbit from which the semi-major axis can be easily computed. Generally, the RAO orbit will have the same right ascension of ascending node and argument of perigee as the target orbit to ensure the main alignment of the orbits is the same. This is more important for RAO orbits with elliptical target orbits. Of the five main orbtial parameters, there now exist three from which the best RAO orbit can be chosen. The semi-major axis

is dependent on N_t and N_r, and the eccentricity and inclination are dependent on the semi-major axis. By varying the RAO eccentricity from the target orbit's eccentricity, the observer will travel in and out of the belt creating the same petals described by the Flower Constellations. Then, varying the RAO inclination from the target orbit's inclination allows the observer to travel over and under the target orbit. These two differences allow the observer to get a 360 degree view of the target orbit. Necessary constraints are then introduced to reduce the number of choices of RAO orbits.

CHAPTER II

CIRCULAR TARGET ORBITS

A. Acceptable Orbits

The first step in determining a RAO orbit is to define the associated circular target orbit. With the target orbit's semi-major axis defined, the RAO orbit's semi-major axis must be defined such that a spacecraft in the RAO orbit must never be more than a predefined distance from the target orbit to ensure observation accuracy. This distance is called $d_{\max}$ which can then be used to bound the semi-major axis of the RAO orbit.

$$a_t - d_{\max} \leq a_r \leq a_t + d_{\max} \tag{2.1}$$

This allows a spacecraft to observe the entire target orbit in the amount of time given by Equation (2.2)

$$N_t = \frac{T_r}{|T_t - T_r|} \qquad \text{or} \qquad N_r = \frac{T_t}{|T_t - T_r|} \tag{2.2}$$

where T_r, T_t are the RAO orbital period and the period of the target orbit, respectively. N_r and N_t represent the number of RAO and target orbital periods completed during the repetition time, respectively.

It is also beneficial to impose a time constraint, $T_{\text{rep}\max}$, that limits the amount of time it takes a spacecraft in the RAO orbit to complete a full observation of the target orbit.

$$N_r\, T_r \leq T_{\text{rep}\max} \tag{2.3}$$

Then substituting Equation (2.2) into Equation (2.3) and solving for T_r provides the

limits for T_r

$$\begin{aligned} &\text{for } T_r < T_t: \qquad T_r \leq \frac{T_t\, T_{\text{rep max}}}{T_t + T_{\text{rep max}}} \\ &\text{for } T_r > T_t: \qquad T_r \geq \frac{T_t\, T_{\text{rep max}}}{-T_t + T_{\text{rep max}}} \end{aligned} \tag{2.4}$$

Lastly, we can solve for a_r in Equation (2.4) using Kepler's Third Law

$$T = 2\pi\sqrt{\frac{a^3}{\mu}} \qquad \rightarrow \qquad a = \sqrt[3]{\mu\left(\frac{T}{2\pi}\right)^2} \tag{2.5}$$

and combine the results with Equation (2.1) to provide the final bounds on a_r.

$$\boxed{\begin{aligned} &\text{for } a_r < a_t: \qquad a_t - d_{\max} \leq a_r \leq \sqrt[3]{\mu\left(\frac{1}{2\pi}\,\frac{T_t\, T_{\text{rep max}}}{T_t + T_{\text{rep max}}}\right)^2} \\ &\text{for } a_r > a_t: \qquad a_t + d_{\max} \geq a_r \geq \sqrt[3]{\mu\left(\frac{1}{2\pi}\,\frac{T_t\, T_{\text{rep max}}}{-T_t + T_{\text{rep max}}}\right)^2} \end{aligned}} \tag{2.6}$$

B. Compatible Orbits

While the method previously described will observe a target orbit effectively, there may exist a situation in which one still wants to observe the entirety of an orbit but also knows of one or more objects in that orbit and wants to make sure the RAO spacecraft will always be in the same position relative to those objects. For example, one may want the RAO spacecraft to always be looking down on these objects or looking away from Earth when viewing them. There exists a subset of acceptable orbits called compatible (or resonant) orbits which can do this.

An orbit is called compatible with respect to a rotating reference frame if there exist two integers, $N_r \in \mathbb{Z}(1)$ and $N_t \in \mathbb{Z}(1)$, satisfying

$$N_r\, T_r = N_t\, T_t = T_{\text{rep}} \tag{2.7}$$

which implies a synchronization between RAO and target orbits.

Once T_r is known, the RAO semi-major axis can be computed using Equation (2.5)

$$a_r = \sqrt[3]{\mu \left(\frac{T_r}{2\pi}\right)^2} = \sqrt[3]{\mu \left(\frac{N_t\, T_t}{2\pi\, N_r}\right)^2} \tag{2.8}$$

Again $T_{\text{rep}\,\max}$ is needed to place an upper bound on the number of the N_r, N_t combinations. From $T_{\text{rep}\,\max}$, we can derive an upper value for the maximum allowable target orbital periods to observe the target orbit once, $N_{t\,\max} = T_{\text{rep}\,\max}/T_t$. Additionally, $d_{\max}$ is still needed to maintain the observation resolution within the requirements of the observation accuracy.

As an example, Figure 4 shows all the possible N_r, N_t combinations of a scenario for which the target orbit is the geostationary orbit whose parameters are defined in Table I.

Table I. Geostationary Orbit Parameters (Example 1)

T_t (hr)	a_t (km)	e_t	Ω_t (deg)	i_t (deg)	ω_t (deg)	$d_{\max}$ (km)	$T_{\text{rep}\,\max}$ (day)
24	42,164	0	0	0	0	5,000	30

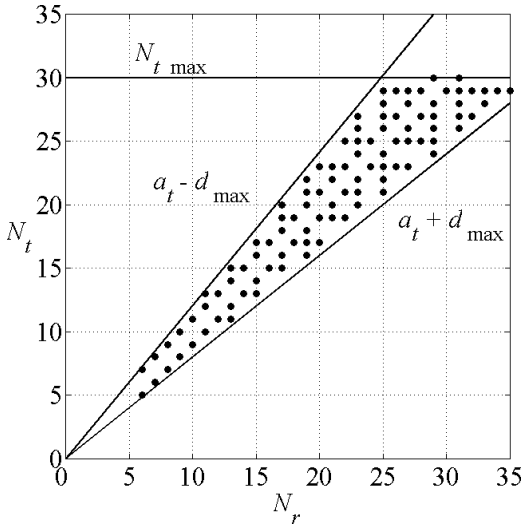

Fig. 4. Compatible Orbits for a Circular Target Orbit (Example 1)

The bounds defined by $d_{\max}$ and $N_{t\max}$ can be seen in Figure 4. It can then be seen that increasing $N_{t\max}$ will increase the number of possible N_r, N_t combinations and decreasing $N_{t\max}$ will lower the number of possible N_r, N_t combinations. The same behavior can be seen for $d_{\max}$.

C. Eccentricity and Inclination Bounds

These orbits in and of themselves are not considered RAO orbits. They are simply circular orbits with an acceptable or compatible period. By making the orbit eccentric and inclined, the orbits can then be considered RAO orbits. For a given target orbit, the minimum and maximum possible apogees and perigees for all RAO orbits will be the same. Using Equation (2.8) to find the semi-major axis, a_r, for all compatible orbits in Figure 4, the eccentricities associated with these minimum and maximum apogees and perigees can then be found. For RAO orbits where $a_r < a_t$, the RAO apogee must be greater than the radius of the target orbit to ensure the "rock-around" motion, and the RAO perigee must be greater than $a_t - d_{\max}$ to ensure it is within

the $d_{\max}$ boundary from the target orbit. Similarly RAO orbits where $a_r > a_t$ must ensure that the perigee is less than the radius of the target orbit and that the apogee is less than $a_t + d_{\max}$.

The equations for the apogee and perigee of a RAO orbit are

$$R_a = a_r\,(1 + e_r) \qquad \text{and} \qquad R_p = a_r\,(1 - e_r) \tag{2.9}$$

whose values can then be used to compute the two values for the minimum and maximum eccentricities for $a_r < a_t$

$$\begin{aligned} a_t = R_a = a_r\,(1 + e_{\min}) \quad &\rightarrow \quad e_{\min} = \frac{a_t}{a_r} - 1 \\ a_t - d_{\max} = R_p = a_r\,(1 - e_{\max}) \quad &\rightarrow \quad e_{\max} = 1 - \frac{a_t - d_{\max}}{a_r} \end{aligned} \tag{2.10}$$

while the minimum and maximum eccentricities for $a_r > a_t$ are

$$\begin{aligned} a_t = R_p = a_r\,(1 - e_{\min}) \quad &\rightarrow \quad e_{\min} = 1 - \frac{a_t}{a_r} \\ a_t + d_{\max} = R_a = a_r\,(1 + e_{\max}) \quad &\rightarrow \quad e_{\max} = \frac{a_t + d_{\max}}{a_r} - 1 \end{aligned} \tag{2.11}$$

Therefore, the RAO eccentricity bounds are

$$\boxed{\begin{aligned} &\text{for } a_r < a_t: \qquad \frac{a_t}{a_r} - 1 \le e_r \le 1 - \frac{a_t - d_{\max}}{a_r} \\ &\text{for } a_r > a_t: \qquad 1 - \frac{a_t}{a_r} \le e_r \le \frac{a_t + d_{\max}}{a_r} - 1 \end{aligned}} \tag{2.12}$$

If $e_{\min} < 0$, set $e_{\min} = 0$; since e cannot be less than zero.

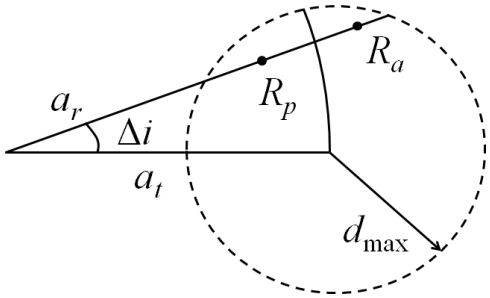

Fig. 5. Inclination Bounds Geometry for a Circular Target Orbit

Inclination bounds are derived from $d_{\max}$ and e_r. Looking at Figure 5, it can be seen that Δi is the inclination difference between the target and RAO orbit. Therefore, the maximum difference is found when R_a or R_p is coincident with the $d_{\max}$ circle. Using the equation of the $d_{\max}$ circle

$$(x - a_t)^2 + y^2 = d_{\max}^2 \tag{2.13}$$

and the two separate possibilities

$$x = R_a \cos i \qquad \text{and} \qquad y = R_a \sin i \tag{2.14}$$

and

$$x = R_p \cos i \qquad \text{and} \qquad y = R_p \sin i \tag{2.15}$$

where R_a and R_p are defined in Equation (2.9), Δi can be found as a function of e_r. Solving the two problems then yields the two possibilities

$$\Delta i(R_a) = \cos^{-1}\left(\frac{d_{\max}^2 - a_r^2\,(1+e_r)^2 - a_t^2}{-2a_r\,(1+e_r)\,a_t}\right) \tag{2.16}$$

$$\Delta i(R_p) = \cos^{-1}\left(\frac{d_{\max}^2 - a_r^2\,(1-e_r)^2 - a_t^2}{-2a_r\,(1-e_r)\,a_t}\right) \tag{2.17}$$

Upon closer examination, it can be found that $i(R_a)$ is valid for $a_r > a_t$ and $i(R_p)$ is valid for $a_r < a_t$.

Hence

$$\boxed{i_{\min} = i_t - \Delta i \leq i_r \leq i_t + \Delta i = i_{\max}} \tag{2.18}$$

where

$$\boxed{\begin{aligned} &\text{for } a_r < a_t: \qquad \Delta i = \cos^{-1}\left(\frac{d_{\max}^2 - a_r^2\left(1-e_r\right)^2 - a_t^2}{-2a_r\left(1-e_r\right)a_t}\right) \\ &\text{for } a_r > a_t: \qquad \Delta i = \cos^{-1}\left(\frac{d_{\max}^2 - a_r^2\left(1+e_r\right)^2 - a_t^2}{-2a_r\left(1+e_r\right)a_t}\right) \end{aligned}} \tag{2.19}$$

Two things are important to note. The first is there are no negative inclinations. If $i_{\min} < 0$, it means the ascending node and descending node have swapped positions which is a 180° change in Ω. So the bounds would be $0 \leq i_r \leq i_{\max}$ for Ω_r and $0 \leq i_r \leq |i_{\min}|$ for $\Omega_r \pm 180°$. The second is that Equations (2.18) and (2.19) are only half right. Using the maximum eccentricity for a RAO orbit would produce $\Delta i = 0°$. If $\omega_r = 0°$ or 180°, the furthest point of the RAO orbit from the target orbit will be the ascending node or descending node. As a spacecraft in the RAO orbit moves away from the node, it will be coming closer to the target orbit and could in fact have some inclination and still be within the $d_{\max}$ boundary.

D. Example

To see how a RAO orbit works, the trajectory of the RAO spacecraft has to be evaluated in the rotating target orbit frame. For this purpose, the coordinate transformation matrices between inertial, rotating target, and RAO orbit frames must be introduced. Using the "3-1-3" Euler's sequence to represent the orientation in space of the orbits, the inertial-to-orbital direction cosine matrix is expressed as

$$C_{i2o} = R_3(\omega + \varphi)\, R_1(i)\, R_3(\Omega) \tag{2.20}$$

where the expressions for the R_1 and R_3 rotation matrices are

$$R_1(\vartheta) = \begin{bmatrix} 1 & 0 & 0 \\ 0 & \cos\vartheta & \sin\vartheta \\ 0 & -\sin\vartheta & \cos\vartheta \end{bmatrix} \qquad \text{and} \qquad R_3(\vartheta) = \begin{bmatrix} \cos\vartheta & \sin\vartheta & 0 \\ -\sin\vartheta & \cos\vartheta & 0 \\ 0 & 0 & 1 \end{bmatrix} \tag{2.21}$$

The inertial-to-RAO (fixed) orbit transformation matrix is

$$C_{i2r} = R_3(\omega_r)\, R_1(i_r)\, R_3(\Omega_r) \tag{2.22}$$

and the inertial-to-target (rotating) orbit transformation matrix is

$$C_{i2t} = R_3(\omega_t + \varphi_t)\, R_1(i_t)\, R_3(\Omega_t) \tag{2.23}$$

where φ represents the true anomaly of a fictitious spacecraft in the target orbit frame.

Equations (2.22) and (2.23) allow us to evaluate the target-to-RAO orbit transformation matrix

$$C_{r2t} = C_{i2t}\, C_{r2i} = C_{i2t}\, C_{i2r}^{\mathrm{T}} \tag{2.24}$$

Therefore, the relative motion of the RAO orbit in the target orbit frame is ruled by

$$R_r^{(t)} = \begin{Bmatrix} x_r^{(t)} \\ y_r^{(t)} \\ z_r^{(t)} \end{Bmatrix} = C_{r2t}\, R_r^{(r)} = C_{i2t}\, R_r^{(i)} \tag{2.25}$$

where $R_r^{(i)}$, $R_r^{(t)}$, and $R_r^{(r)}$, indicate the RAO position vector as expressed in the inertial, target, and RAO reference frames, respectively.

Using the geostationary orbit (whose parameters are defined in Table I) as a target orbit, let us now consider two RAO orbits, whose derived orbital parameters are provided in Table II and whose example orbital parameters are provided in Table III.

Table II. Derived RAO Orbital Parameters (Example 1)

Scenario	N_r	N_t	T_r (hr)	a_r (km)	$e_{r\,\min}$	$e_{r\,\max}$
1	25	24	22.98	$41,032$	0.0276	0.0943
2	24	25	24.93	$43,327$	0.0268	0.0886

Table III. Selected RAO Orbital Parameters (Example 1)

Scenario	e_r	Ω_r (deg)	i_r (deg)	ω_r (deg)
1	0.0943	0	5.75	0
2	0.0886	0	5.75	0

Figure 6 shows the GEO and RAO orbits as projected on the GEO reference plane for the two RAO scenarios selected. Figure 7 shows the GEO and the RAO orbits as appearing in the rotating GEO reference frame (top view) while Figure 8 shows the same orbits as given in Figure 7 in a fixed 3D view.

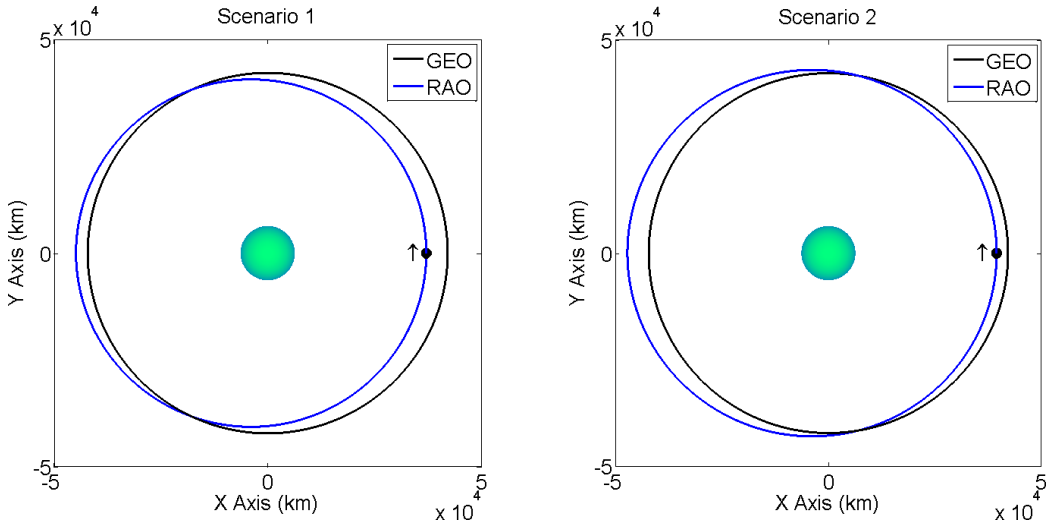

Fig. 6. GEO and RAO Orbits in the Inertial Frame (Example 1)

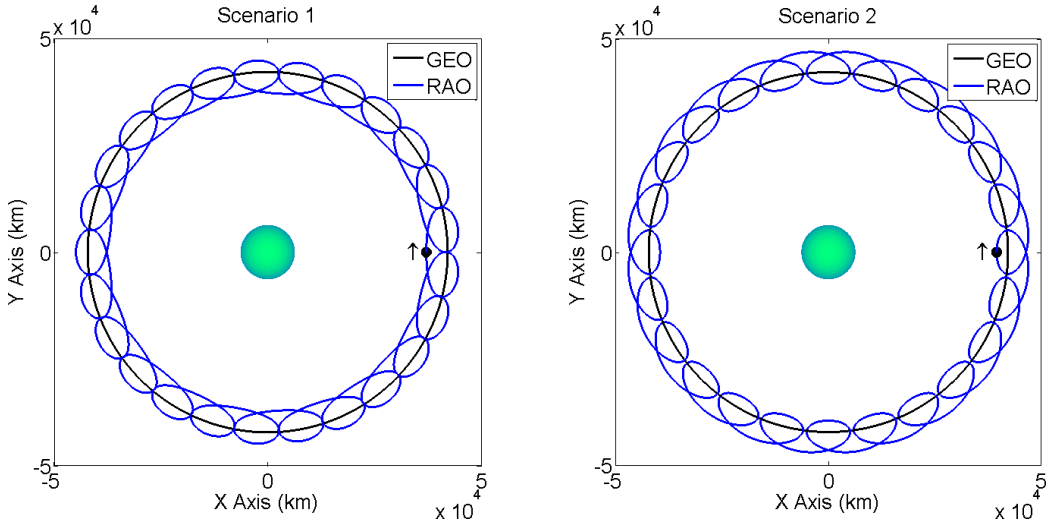

Fig. 7. GEO and RAO Orbits in the Rotating GEO Frame: Top View (Example 1)

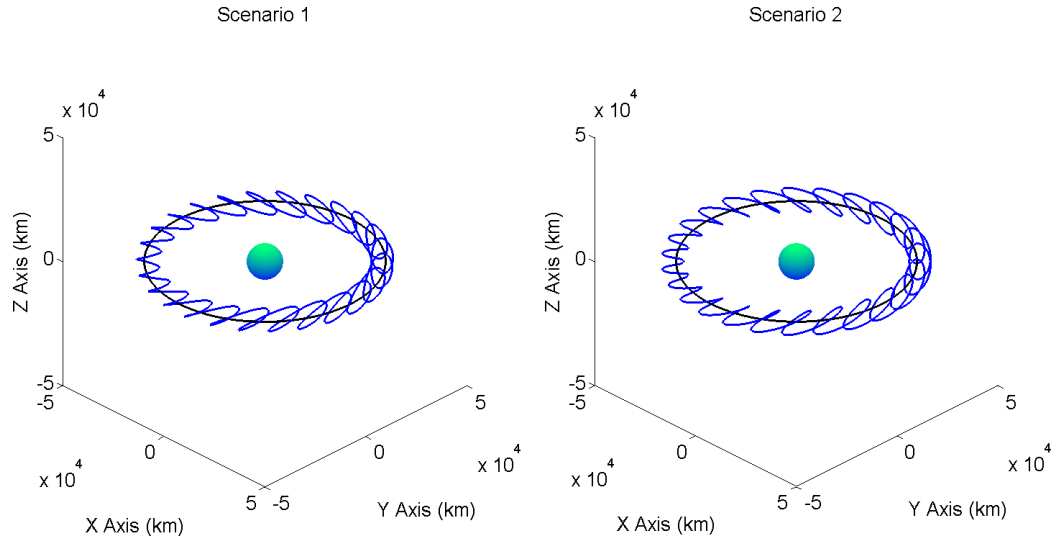

Fig. 8. GEO and RAO Orbits in the Rotating GEO Frame: Fixed 3D View (Example 1)

Both of the RAO orbits have "petals" in which the observer covers a portion of the GEO belt twice. The number of these is controlled by the $[N_r, N_t]$ combination chosen from Figure 4. The size of the petals can be increased or decreased by changing the eccentricity and the inclination of the RAO orbit. It is also of interest to note that the RAO orbit with a semi-major axis greater than that of the GEO belt spends more time outside the belt than inside, and the opposite occurs for the RAO orbit with a semi-major axis smaller than that of the GEO belt.

E. Minimum Distance

Knowing the minimum distance, $D_{\min}$, from the RAO spacecraft to the target orbit is a useful tool. To find $D_{\min}$, the RAO trajectory must be evaluated in the fixed, not rotating, target frame. Therefore we have to rewrite Equation (2.23) as

$$C_{i2t} = R_3(\omega_t)\, R_1(i_t)\, R_3(\Omega_t) \tag{2.26}$$

Then using Equations (2.22), (2.26), (2.24), and (2.25), we can get the RAO trajectory in the fixed target orbit reference frame. From this, the projection of the RAO values onto the target orbit plane gives the vector $\{\, x_r^{(t)},\ y_r^{(t)},\ 0\,\}^{\mathrm{T}}$. The distance between the projection and the target orbit is simply the radial distance to the projection minus the radius of the target orbit. This new segment combined with R_r and $D_{\min}$ form a right triangle with $D_{\min}$ as the hypotenuse. Therefore, $D_{\min}$ can be found using the Pythagorean theorem. The diagram can be seen in Figure 9.

$$D_{\min} = \sqrt{\left(\sqrt{\left(x_r^{(t)}\right)^2 + \left(y_r^{(t)}\right)^2} - a_t\right)^2 + \left(z_r^{(t)}\right)^2} \tag{2.27}$$

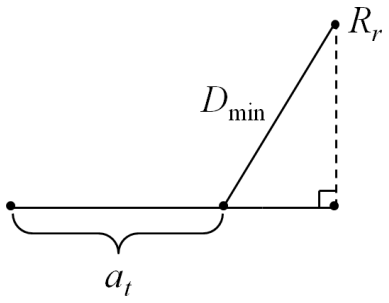

Fig. 9. Diagram of Minimum Distance from Spacecraft to Circular Target Orbit

Figure 10 provides the minimum distance between the RAO and GEO orbits in one RAO orbital period. As can be seen, the RAO orbit is always within the $d_{\max}$ boundary while using the maximum eccentricity and an inclination greater than zero.

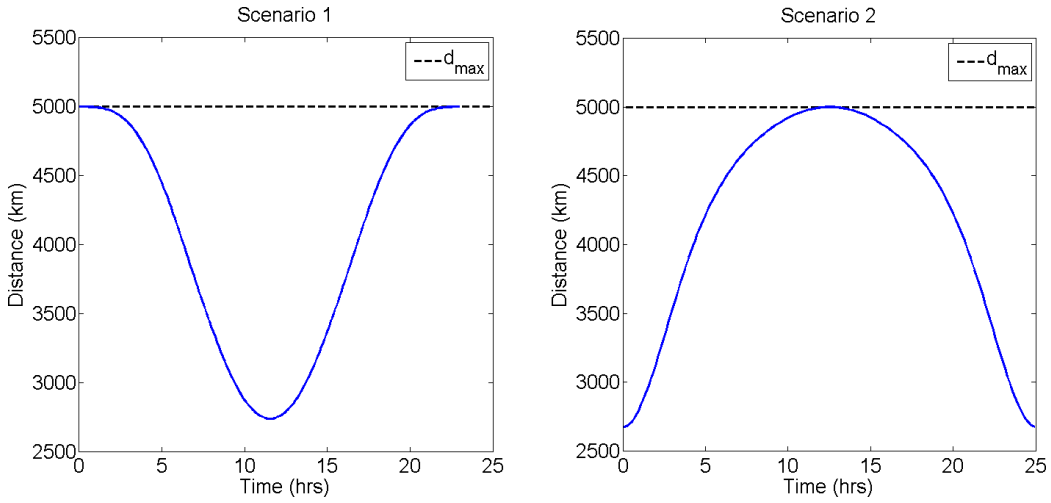

Fig. 10. Minimum Distance between RAO and GEO Orbits for One RAO Orbital Period (Example 1)

CHAPTER III

ELLIPTICAL TARGET ORBITS

Finding RAO orbits for elliptical target orbits is slightly different than circular target orbits since the eccentricity of the target orbit is no longer a constant.

A. Acceptable and Compatible Orbits

The process for finding acceptable and compatible orbits is the same as described in Chapter II. The target orbit parameters in this example are shown in Table IV and a graph of its compatible orbits in Figure 11.

Table IV. Elliptical Target Orbit Parameters (Example 2)

T_t (hr)	a_t (km)	e_t	Ω_t (deg)	i_t (deg)	ω_t (deg)	$d_{\max}$ (km)	$N_{d_{\max}}$ (day)
22.12	40,000	0.5	0.0	0.0	0.0	5,000	30

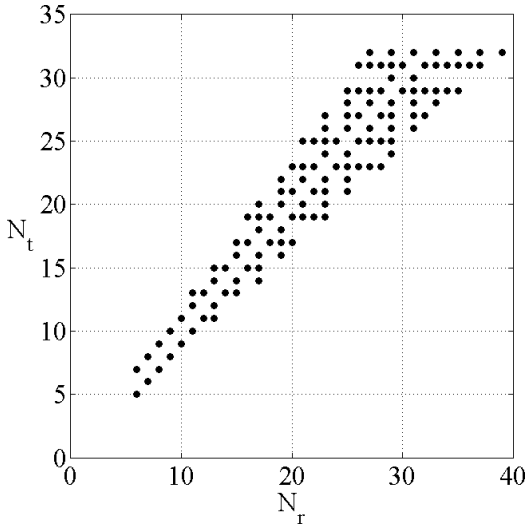

Fig. 11. Compatible Orbits for Elliptical Target Orbit (Example 2)

B. Eccentricity and Inclination Bounds

It is here that the process differs from Chapter II. Since the apogee and perigee are the extrema of the target orbit, the RAO orbit should be no farther than $d_{\max}$ from these points. Using Equation (2.9) and solving it for the minimum and maximum eccentricities yields

$$\begin{aligned} &\text{for } a_r < a_t: \qquad e_2 = \frac{R_a - d_{\max}}{a_r} - 1 \leq e_r \leq 1 - \frac{R_p - d_{\max}}{a_r} = e_4 \\ &\text{for } a_r > a_t: \qquad e_3 = 1 - \frac{R_p + d_{\max}}{a_r} \leq e_r \leq \frac{R_a + d_{\max}}{a_r} - 1 = e_1 \end{aligned} \tag{3.1}$$

The eccentricity bounding values, e_1 through e_4, as provided by Equation (3.1) are plotted in Figure 12 for a large range of semi-major axes.

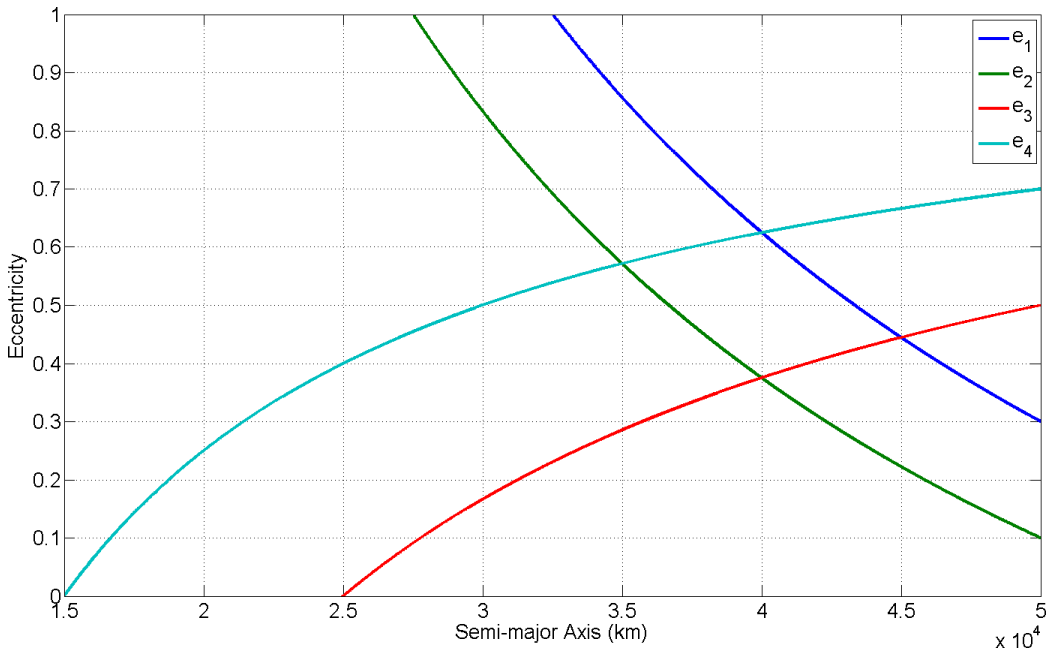

Fig. 12. RAO Eccentricity Bounds for $d_{\max}$ as a Function of the Semi-major Axis (Example 2)

The results of zooming in on Figure 12 and plotting the semi-major axes from Figure 11, which are the vertical black lines, can be seen in Figure 13. The effects of $d_{\max}$ and $N_{t\max}$ are also apparent in Figure 13. Increasing $d_{\max}$ causes the different e lines to move away from the center and thus increases the area between them. Decreasing $d_{\max}$ causes the e lines to constrict, decreasing the area between them. Increasing $N_{t\max}$ will produce two effects. The first will obviously increase the number of possible semi-major axes. The second is that some of these new semi-major axes will have periods closer to that of the target orbit therefore allowing more semi-major axes closer to that of the target orbit which are seen as more lines closer to the target semi-major axis. Decreasing $N_{t\max}$ will have the opposite result for both influences.

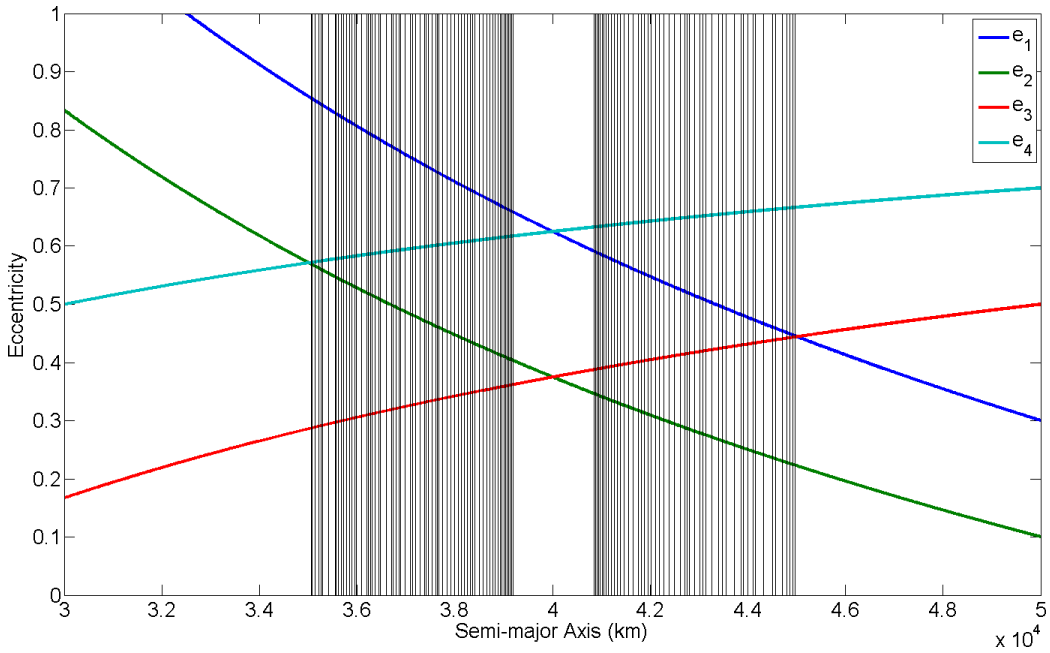

Fig. 13. RAO Eccentricity Bounds for $d_{\max}$ with the Compatible Semi-major Axes (Example 2)

The next step is to determine the best eccentricity for each of the RAO semi-major axes. Figure 14 is a contour plot in which the x and y axes are the same as in Figure 13, but the z axis is the percentage of time that a spacecraft in the associated RAO orbit is within the $d_{\max}$ boundary of the target orbit for which $i_t = i_r$. Nearly all of the area defined by the four intersections of the eccentricities has a 100% rating. The eccentricities e_1, e_3, and their intersection along with e_2, e_4, and their intersection bound the two regions where the RAO spacecraft is never within range of the target orbit. The 100% region will become more tightly bounded as the target orbit's eccentricity decreases until it is zero at which point it is completely bounded by e_1 and e_2. The opposite happens when the eccentricity of the target orbit increases allowing more results with a percentage rating of less than 100% into the area defined by the four intersections of the eccentricities. These effects can be seen in Appendix A.

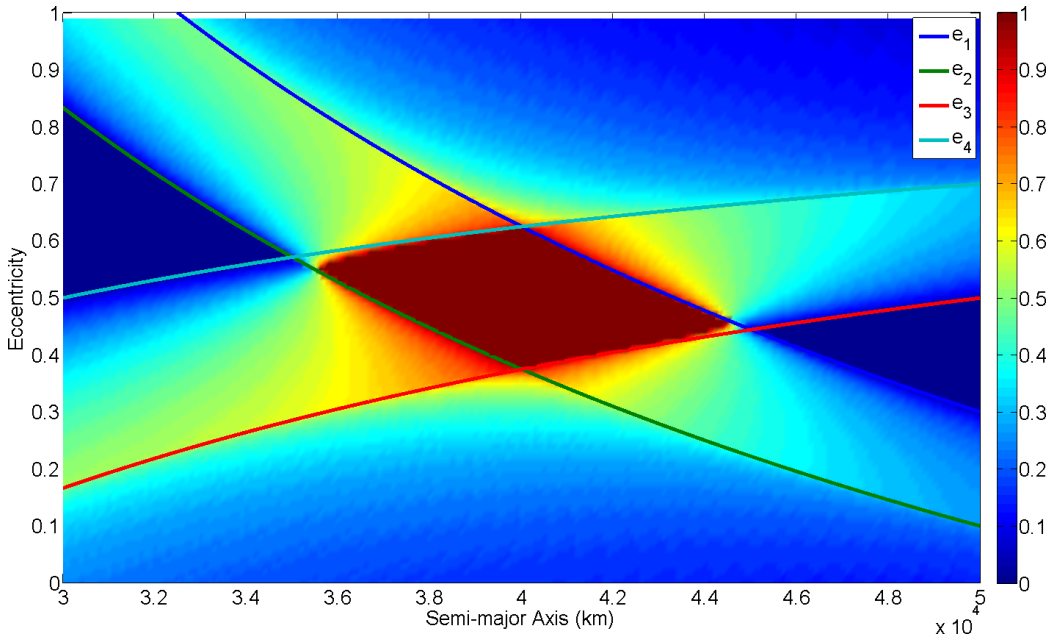

Fig. 14. Percentage of Time a Spacecraft in a RAO Orbit is within $d_{\max}$ of the Target Orbit (Example 2)

Regardless, this still leaves a large range of eccentricity values for some of the RAO semi-major axes. Even though the target and RAO orbits are both eccentric, the RAO eccentricity must vary enough from the target orbit's eccentricity to have the "rock-around" motion just like in the Circular Target Orbits section. Using Equation (2.9) and solving it for the eccentricities needed for "rock-around" motion provides

$$e_5 = \frac{R_a}{a_r} - 1 \qquad \text{and} \qquad e_6 = 1 - \frac{R_p}{a_r} \tag{3.2}$$

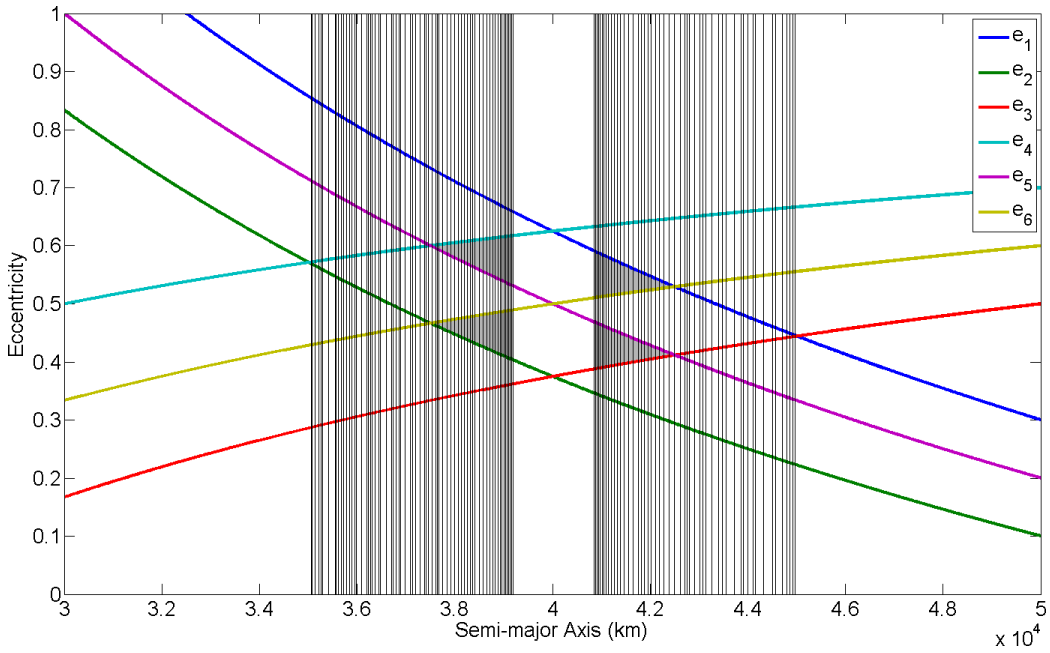

Fig. 15. All RAO Eccentricity Bounds and Valid Solutions (Example 2)

Using the data in Figure 13 and including Equation (3.2), Figure 15 shows several interesting and important features. For a RAO orbit with an elliptical target orbit one of two conditions must apply to ensure "rock-around" motion: the RAO apogee must be greater than the target apogee and the RAO perigee smaller than the target perigee, or the RAO apogee must be smaller than the target apogee and the RAO

perigee greater than the target perigee. For $a_r < a_t$, this can be seen above e_5 and below e_6; and for $a_r > a_t$, this applies above e_6 and below e_5. Of the 100% region from Figure 14, only the shaded areas in Figure 15 exhibit "rock-around" motion. This removes many of the possible semi-major axes and reduces the eccentricity range of those that remain.

Using Figures 14 and 15 and combining Equations (3.1) and (3.2), the final piecewise eccentricity bounds for an elliptical target orbit can be constructed.

$$\begin{array}{lll}
\text{for } a_r < a_t: & \dfrac{R_a - d_{\max}}{a_r} - 1 \leq e_r \leq 1 - \dfrac{R_p}{a_r} & \\
\text{and} & \dfrac{R_a}{a_r} - 1 \leq e_r \leq 1 - \dfrac{R_p - d_{\max}}{a_r} & \\
\text{for } a_r > a_t: & 1 - \dfrac{R_p + d_{\max}}{a_r} \leq e_r \leq \dfrac{R_a}{a_r} - 1 & \\
\text{and} & 1 - \dfrac{R_p}{a_r} \leq e_r \leq \dfrac{R_a + d_{\max}}{a_r} - 1 &
\end{array} \tag{3.3}$$

The inclination bounds differ from RAO orbits with circular target orbits because the target orbit does not have a fixed radius. Looking at Figure 16, it can be seen that there are two possible Δi values, one associated with the apogee and one associated with the perigee of the target orbit.

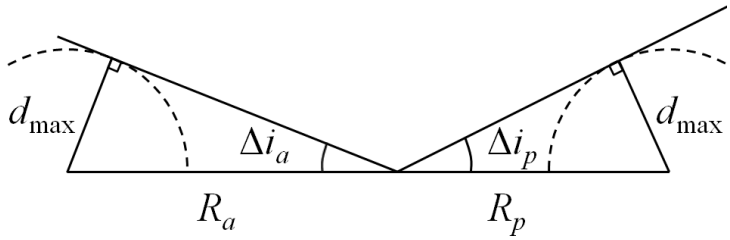

Fig. 16. Inclination Bounds Geometry for an Elliptical Reference Orbit

Since $R_a > R_p$, it follows that $\Delta i_a < \Delta i_p$. Now we have to choose whether Δi_a or Δi_p will become Δi. Using Δi_a ensures that the spacecraft in the RAO orbit will be within the $d_{\max}$ boundary over the whole target orbit including the perigee whereas using Δi_p would allow the spacecraft to travel out of the $d_{\max}$ boundary over the target orbit's apogee; hence $\Delta i = \Delta i_a$. Substituting R_a of the target orbit into a_t of Equation (2.19) provides the inclination bounds.

$$\boxed{i_{\min} = i_t - \Delta i \leq i_r \leq i_t + \Delta i = i_{\max}} \tag{3.4}$$

where

$$\boxed{\begin{aligned} &\text{for } a_r < a_t: \qquad \Delta i = \cos^{-1}\left(\frac{d_{\max}^2 - a_r^2\left(1-e_r\right)^2 - a_t^2}{-2a_r\left(1-e_r\right)a_t\left(1+e_t\right)}\right) \\ &\text{for } a_r > a_t: \qquad \Delta i = \cos^{-1}\left(\frac{d_{\max}^2 - a_r^2\left(1+e_r\right)^2 - a_t^2}{-2a_r\left(1+e_r\right)a_t\left(1+e_t\right)}\right) \end{aligned}} \tag{3.5}$$

C. Example

In this example, we will look at an elliptical target orbit and a RAO orbit whose parameters can be found in Tables V, VI, and VII. Looking at Figure 17, the target and RAO orbit can be seen in the inertial and rotating frame. The target orbit belt does not remain fixed like a circular target orbit in the rotating frame since $\varphi \neq M$ all the time for an elliptical orbit. This can make it difficult to understand the RAO spacecraft motion in the target orbit reference frame. One alternative way to think about it is when the RAO satellite is at its apogee, it is surveying all the spacecraft in the target orbit that are at or near apogee and similarly so for perigee. Another way to think about it is to realize that since $N_r = 14$, the RAO spacecraft will cover 1/14 of the target orbit in one RAO period.

Table V. Elliptical Target Orbit Parameters (Example 3)

T_t (hr)	a_t (km)	e_t	Ω_t (deg)	i_t (deg)	ω_t (deg)	$d_{\max}$ (km)	$N_{d_{\max}}$ (day)
22.12	40,000	0.1	0.0	0.0	0.0	5,000	30

Table VI. Derived RAO Orbital Parameters (Example 3)

T_r (hr)	a_r (km)	$e_{r\,\min}$	$e_{r\,\max}$	$e_{r\,\min}$	$e_{r\,\max}$
20.54	38,072	0.0244	0.0544	0.1557	0.1857

Table VII. Selected RAO Orbital Parameters (Example 3)

e_r	Ω_r (deg)	i_r (deg)	ω_r (deg)
0.1857	0	4.75	0

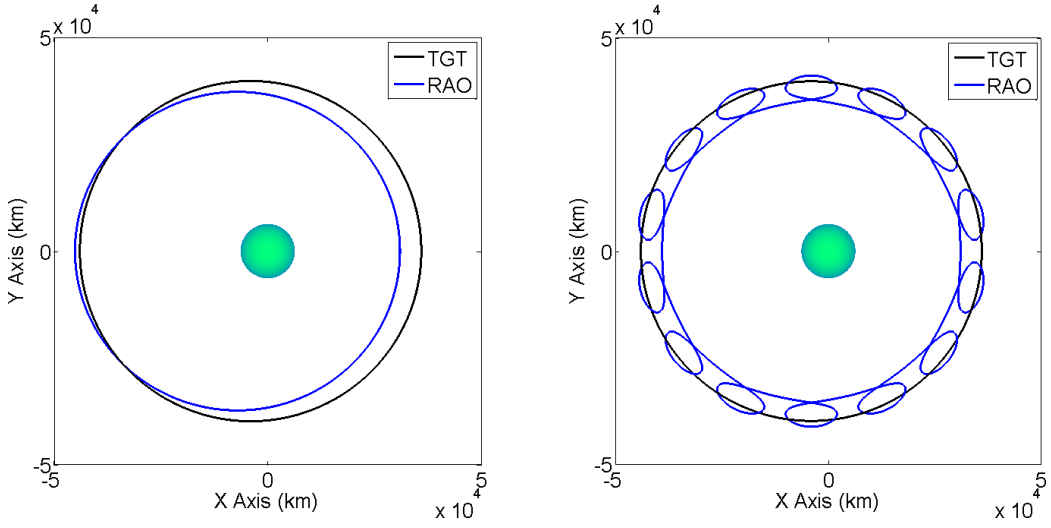

Fig. 17. TGT and RAO Orbits in the Inertial Frame and Rotating $\dot{M}_t$ Frame (Example 3)

D. Minimum Distance

Like the calculation of minimum distance in Chapter II, the RAO orbit's position needs to be found in the target orbit's reference frame. However, the RAO orbit's inertial shape should still be maintained. Therefore, Equation (2.20) becomes

$$C_{i2o} = R_3(\omega)\, R_1(i)\, R_3(\Omega) \tag{3.6}$$

leaving out the true anomaly and preserving the orbit's true elliptical form. The other transformation matrices can be derived from this new base equation.

The process also differs here, since the target orbit is now elliptical requiring a new approach to solve D_{min}. From here on, no orbital mechanics are used; so the orbits will be defined as ellipses in their geometric and parametric forms. The rest of this problem will assume the target orbit reference frame has the target orbit centered at the origin, not the focus. This translation can be seen in Figure 18. Therefore, the trajectory of the RAO orbit in the translated target orbit reference frame is now

$$R_r^{(t)} = C_{i2t} R_r^{(i)} + \{\, a_t\, e_t,\ 0,\ 0 \,\}^{\mathrm{T}} \tag{3.7}$$

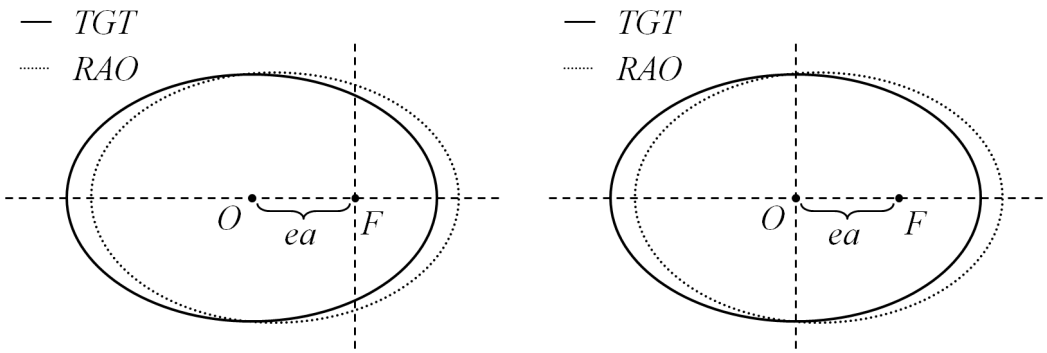

Fig. 18. TGT and RAO Ellipses before and after *ea* Translation

At this point, we will now find the distance from a point to the ellipse in 2D [9]. Let any point on the RAO orbit's projection $(x_r^{(t)}, y_r^{(t)})$ as defined in Equation (3.7) now be called (u, v), and then the target orbit be defined as

$$\left(\frac{x}{a}\right)^2 + \left(\frac{y}{b}\right)^2 = 1 \tag{3.8}$$

where $a = a_t$ and $b = b_t$ are the semi-major and semi-minor axes of the target orbit, respectively. The minimum distance from (u, v) to the ellipse must be such that $(u - x, v - y)$ lie on the normal of the ellipse at the closest point. The normal of the ellipse is

$$\nabla\left(\left(\frac{x}{a}\right)^2 + \left(\frac{y}{b}\right)^2 - 1\right) = \left(\frac{2x}{a^2}\,,\,\frac{2y}{b^2}\right) \tag{3.9}$$

Therefore

$$(u - x, v - y) = t\left(\frac{x}{a^2}\,,\,\frac{y}{b^2}\right) \tag{3.10}$$

for some t. Solving for x and y in Equation (3.10) yields

$$x = \frac{a^2 u}{t + a^2} \qquad \text{and} \qquad y = \frac{b^2 v}{t + b^2} \tag{3.11}$$

For any (u, v), the closest point (x, y) will lie in the same quadrant since both points lie on the same line normal to the ellipse meaning u and x must have the same sign as well as v and y. Therefore the constraints on t are $t > -a^2$ and $t > -b^2$. Since $a > b$, the only constraint is $t > -b^2$. Substituting Equation (3.11) into Equation (3.8) yields.

$$F(t) = \left(\frac{au}{t + a^2}\right)^2 + \left(\frac{bv}{t + b^2}\right)^2 - 1 = 0 \tag{3.12}$$

Since $F(t)$ is a quartic polynomial, there are four values for t. To determine which value is the correct one, we will look at the graphs of $F(t)$ to help. There are three possibilities for the graph of $F(t)$ which depend on where (u, v) is located with

respect to the evolute of the ellipse which can be defined parametrically as

$$x = \frac{a^2 - b^2}{a}\cos^3 t \qquad \text{and} \qquad y = \frac{b^2 - a^2}{b}\sin^3 t \tag{3.13}$$

The three possibilities can be seen in Figure 19 and their corresponding graphs of $F(t)$ in Figure 20 where (u, v) lies inside, on, and oustide the evolute, respectively.

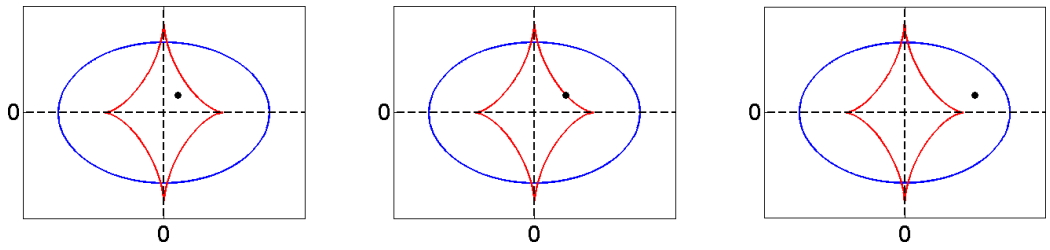

Fig. 19. Ellipse and Evolute with (u, v) inside, on, and outside the Evolute

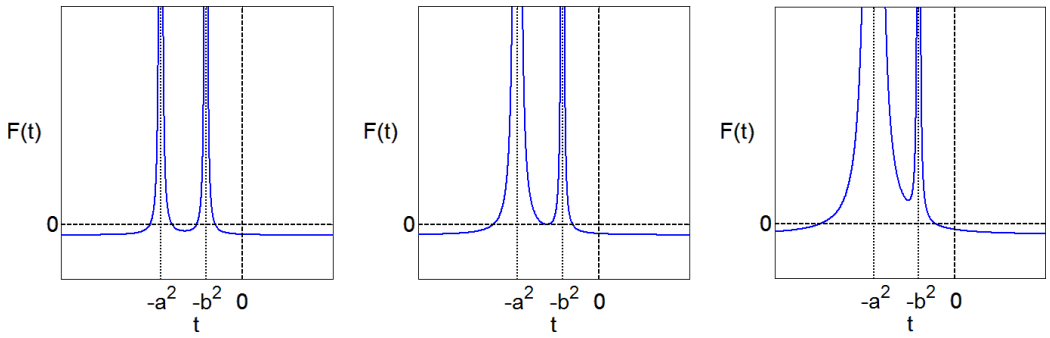

Fig. 20. $F(t)$ for (u, v) inside, on, and outside the Evolute

Of the four roots, the largest real root is always the only one greater than $-b^2$ as can be seen in Figure 20. Substituting this value of t back into Equation (3.11), we can find the closest point on the ellipse to (u, v). Using the known values and Figure 21, a triangle can be constructed and $D_{\min}$ found using the Pythagorean theorem

$$D_{\min} = \sqrt{(u - x)^2 + (v - y)^2 + z_r^{(t)^2}} \tag{3.14}$$

where $(u, v) = (x_r^{(t)}, y_r^{(t)})$ and (x, y) are defined in Equation (3.11) where t is the largest real root of Equation (3.12).

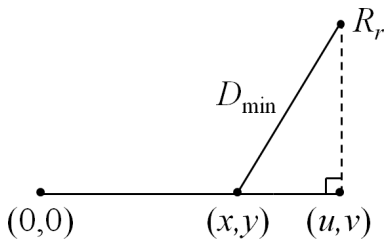

Fig. 21. Diagram of Minimum Distance from Spacecraft to Elliptical Target Orbit

Figure 22 provides the minimum distance between the RAO and target orbits in one RAO orbital period. The orbital parameters can be found in Tables V, VI, and VII. As it can be seen, the distance between the two orbits reaches but never exceeds $d_{\max}$ even with the maximum eccentricity and an inclination.

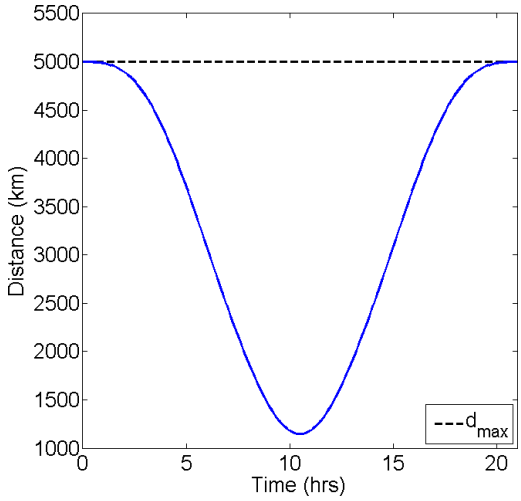

Fig. 22. Minimum Distance between RAO and TGT Orbits for One RAO Orbital Period (Example 3)

CHAPTER IV

J_2 PERTURBATIONS

The Rock-Around Orbit theory so far presented is based on the Keplerian two-body problem. Unfortunately, perturbations do exist and can destroy the RAO relative trajectory if the effects of the perturbations are different on the RAO orbit than on the target orbit. As a first simplified model (linear J_2), let us consider two distinct effects: the nodal precession rate ($\dot{\Omega}$) and the argument of perigee rate ($\dot{\omega}$) differences. When these variations cannot be set to zero, control is needed for orbit maintenance. This section summarizes the linear effect of J_2 on Ω and ω that will be used for the next section on orbit maintenance.

The main effects of the linear J_2 perturbations are the variation of the right ascension of ascending node

$$\frac{d\Omega}{dt} = -\frac{3}{2} J_2 \left(\frac{R_e}{p}\right)^2 n \cos i \tag{4.1}$$

and the variation of the argument of perigee

$$\frac{d\omega}{dt} = \frac{3}{4} J_2 \left(\frac{R_e}{p}\right)^2 n \left(5\cos^2 i - 1\right) \tag{4.2}$$

where

$$n = \frac{dM}{dt} = n_0 \left[1 + \frac{3}{4} J_2 \left(\frac{R_e}{p}\right)^2 \left(2 - 3\sin^2 i\right) \sqrt{1-e^2}\right] \tag{4.3}$$

is the perturbed mean motion, n_0 the unperturbed mean motion, R_e the Earth's radius, and p the semi-latus rectum.

Using these equations, we can find the correct semi-major axis, eccentricity, and inclination combination that will allow $\dot{\Omega}_r$ and $\dot{\omega}_r$ to equal or be near those values of the target orbit thus preserving the shape of the relative orbit and reducing station-

keeping fuel requirements.

A. Right Ascension of Ascending Node (Ω) Maintenance

We want to have a RAO orbit with a Ω precession as close to that of the target orbit to minimize the Δv needed to keep the orbits aligned. The first step is determining the rate difference, $\dot{\Omega}_d$, between the two precession rates.

$$\dot{\Omega}_d = \dot{\Omega}_t - \dot{\Omega}_r \tag{4.4}$$

Using the constant time variation, a time length Δt needs to be determined for which the angular precession can be determined.

$$\Delta\Omega_d = \dot{\Omega}_d \, \Delta t \tag{4.5}$$

The first part of the Ω orbit correction is performed at one of the antinodes of the perturbed orbit where $\omega + \varphi = 90^\circ$ or 270°. The antinode with a smaller velocity should be used to minimize the Δv. Therefore, we need to find the velocity at the antinode. This can be done using the radius at that point

$$r = \frac{p}{1 + e\cos\varphi} \tag{4.6}$$

and the vis viva (or energy) equation

$$v = \sqrt{\mu\left(\frac{2}{r} - \frac{1}{a}\right)} \tag{4.7}$$

Looking at Equation (4.1), it can be seen that $\dot{\Omega}_d$ will be negative for $-90^\circ < i_r < 90^\circ$ and positive for $90^\circ < i_r < 270^\circ$. In Figure 23, we show a spherical triangle for the two different cases. Using the spherical law of sines and cosines, we can find $\Delta\vartheta$ which

happens to be the same for both cases.

$$\Delta\vartheta = \tan^{-1}\left(\sin i \, \tan \Delta\Omega\right) \tag{4.8}$$

With $\Delta\vartheta$ and v computed, the first impulse for the correction is

$$\Delta v_1 = 2\, v_{\text{anti}} \, \sin\left(\frac{\Delta\vartheta}{2}\right) \tag{4.9}$$

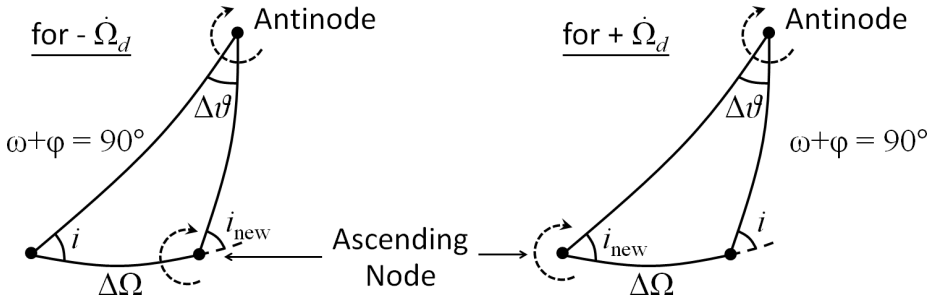

Fig. 23. Spherical Triangle Geometry

This impulse brings the ascending node back to its original position but has changed the orbit's inclination. Using $\vec{r}$ and $\vec{v}_{\text{new}}$ at the antinode, we can compute the orbital elements of the new orbit including the new inclination, i_{new}. Then, v can be found at the ascending and descending node, $\omega + \varphi = 0^\circ$ and 180°, respectively, using Equations (4.6) and (4.7). The correction should be performed at whichever has node has the smaller v. With these values, Δv_2 can now be determined.

$$\Delta v_2 = 2\, v_{\text{node}} \, \sin\left(\frac{|i - i_{\text{new}}|}{2}\right) \tag{4.10}$$

Lastly the total cost, Δv_Ω, is simply

$$\Delta v_\Omega = \Delta v_1 + \Delta v_2 \tag{4.11}$$

This process for finding the Δv of $\dot{\Omega}_d$ assumes that the spacecraft in the target orbit are not performing corrections to maintain their original orbit. If spacecraft in

the target orbit are correcting their orbit, then Δv should be found for just $\dot{\Omega}_r$. This will give the Δv needed to maintain the RAO orbit.

B. Argument of Perigee (ω) Maintenance

Just like the previous section, the difference between the rate of precession of ω for the target orbit and RAO orbit must be found.

$$\dot{\omega}_d = \dot{\omega}_t - \dot{\omega}_r \tag{4.12}$$

And similarly, a time length Δt needs to be determined for which the angular precession can be determined.

$$\Delta\omega_d = \dot{\omega}_d \, \Delta t \tag{4.13}$$

From Lagrange's planetary equations, the rate of change of the argument of perigee is

$$\frac{d\omega}{dt} = -\frac{\sqrt{1-e^2}\cos\varphi}{nae} a_r + \frac{p\sin\varphi}{eh}\left(\frac{2+e\cos\varphi}{1+e\cos\varphi}\right) a_t - \frac{r\cot i \sin(\omega+\varphi)}{na^2\sqrt{1-e^2}} a_n \tag{4.14}$$

where (a_r, a_t, a_n) are the perturbing accelerations acting on the satellite in the radial, tangential, and normal to the orbit plane directions, respectively. The argument of perigee can be corrected by either applying a tangential thrust at the semi-latus rectum ($\varphi = 90^\circ$ or 270°) or a radial thrust at the perigee or apogee ($\varphi = 0^\circ$ or 180°). The tangential thrust uses half as much fuel as the radial method but changes the orbit semi-major axis and eccentricity, which must then be corrected. Thrust applied in the normal direction does not significantly contribute to the ω correction.

Using the acceleration in the tangential direction and evaluating it at the semi-latus rectum, we can get the equation

$$\frac{d\omega}{dt} = \frac{p\sin\varphi}{eh}\left(\frac{2+e\cos\varphi}{1+e\cos\varphi}\right)a_t \;\rightarrow\; \left.\frac{d\omega}{dt}\right|_{90^\circ} = \frac{2p}{eh}a_t \;\rightarrow\; d\omega = \frac{2p}{eh}a_t dt = \frac{2p}{eh}dv \quad (4.15)$$

which can then be discretized and solved for Δv.

$$\Delta\omega_d = \left(\frac{2p}{eh}\right)\Delta v = \left(\frac{2}{e}\sqrt{\frac{p}{\mu}}\right)\Delta v \;\rightarrow\; \Delta v = \left(\frac{e}{2}\sqrt{\frac{\mu}{p}}\right)\Delta\omega_d \quad (4.16)$$

The same method can be used in the radial direction and evaluated at the apogee which gives

$$\frac{d\omega}{dt} = -\frac{\sqrt{1-e^2}}{nae}\cos\varphi\, a_r \;\rightarrow\; \left.\frac{d\omega}{dt}\right|_{180^\circ} = \frac{\sqrt{1-e^2}}{nae}a_r \;\rightarrow\; d\omega = \frac{\sqrt{1-e^2}}{nae}dv \quad (4.17)$$

which can then be discretized and solved for Δv.

$$\Delta\omega_d = \frac{\sqrt{1-e^2}}{nae}\Delta v = \frac{1}{e}\sqrt{\frac{a(1-e^2)}{\mu}}\Delta v = \left(\frac{1}{e}\sqrt{\frac{p}{\mu}}\right)\Delta v \;\rightarrow\; \Delta v = \left(e\sqrt{\frac{\mu}{p}}\right)\Delta\omega_d \quad (4.18)$$

Therefore, the Δv for ω maintenance is

$$\boxed{\begin{aligned} \text{for tangential :} \qquad \Delta v_\omega &= \left(\frac{e}{2}\sqrt{\frac{\mu}{p}}\right)\Delta\omega_d \\ \text{for radial :} \qquad \Delta v_\omega &= \left(e\sqrt{\frac{\mu}{p}}\right)\Delta\omega_d \end{aligned}} \quad (4.19)$$

This process for finding the Δv of $\dot{\omega}_d$ also assumes that the spacecraft in the target orbit are not performing corrections to maintain their original orbit. If spacecraft in the target orbit are correcting their orbit, then Δv should be found for just $\dot{\omega}_r$.

There also exist two inclinations for which $\dot{\omega} = 0$. Using the latter part of Equation (4.2) and setting it equal to zero yields the critical inclinations. Since the cosine is squared, the negative sign from $\cos(\pi \pm i)$ is nulled

$$5\cos^2 i_{cr} - 1 = 0 \;\rightarrow\; i_{cr} = \cos^{-1}\left(\frac{1}{\sqrt{5}}\right) \text{ and } i_{cr} = \pi - \cos^{-1}\left(\frac{1}{\sqrt{5}}\right) \tag{4.20}$$

$$i_{cr} = 63.43^\circ \text{ and } 116.57^\circ \tag{4.21}$$

C. Maintenance-Free RAO Orbits

It is also possible to create a RAO orbit such that $\dot{\Omega}_r = \dot{\Omega}_t$ and $\dot{\omega}_r = \dot{\omega}_t$. Using Equations (4.1) and (4.2) and setting them equal to zero provides

$$\begin{aligned} F_1(a,e,i) &= 0 = -\frac{3}{2}J_2\left(\frac{R_e}{p_r}\right)^2 n_r \cos i_r - \dot{\Omega}_t \\ F_2(a,e,i) &= 0 = \frac{3}{4}J_2\left(\frac{R_e}{p_r}\right)^2 n_r \left(5\cos^2 i_r - 1\right) - \dot{\omega}_t \end{aligned} \tag{4.22}$$

Using these two equations together in a minimization routine will yield the (a, e, i) combinations needed for this type of orbit. However the correct combination may lie outside the bounds of one or more of the variables thus prohibiting the use of this orbit.

D. Example

Using the values provided in Table VII, the angular rate differences of the RAO orbit and the Δv needed to maintain them for two different time periods are found in Table VIII. Figures 24, 25, and 26 show the different Δv_Ω, Δv_ω, and Δv_{tot} values, respectively, for all the possible RAO eccentricity and inclination possibilities from Tables VI with respect to the target orbit defined in Table V.

Table VIII. Angular Rate Differences and Δv (Example 3)

		T_r (20.54 hrs)	T_{rep} (11.98 days)
$\dot{\Omega}_d$	(deg/day)	0.00403	0.00403
$\Delta\Omega_d$	(deg)	0.00345	0.0483
Δv_Ω	(m/s)	0.0176	0.246
$\dot{\omega}_d$	(deg/day)	-0.00783	-0.00783
$\Delta\omega_d$	(deg)	-0.00670	-0.0983
Δv_ω	(m/s)	0.0715	1.00
Δv_{tot}	(m/s)	0.0891	1.25

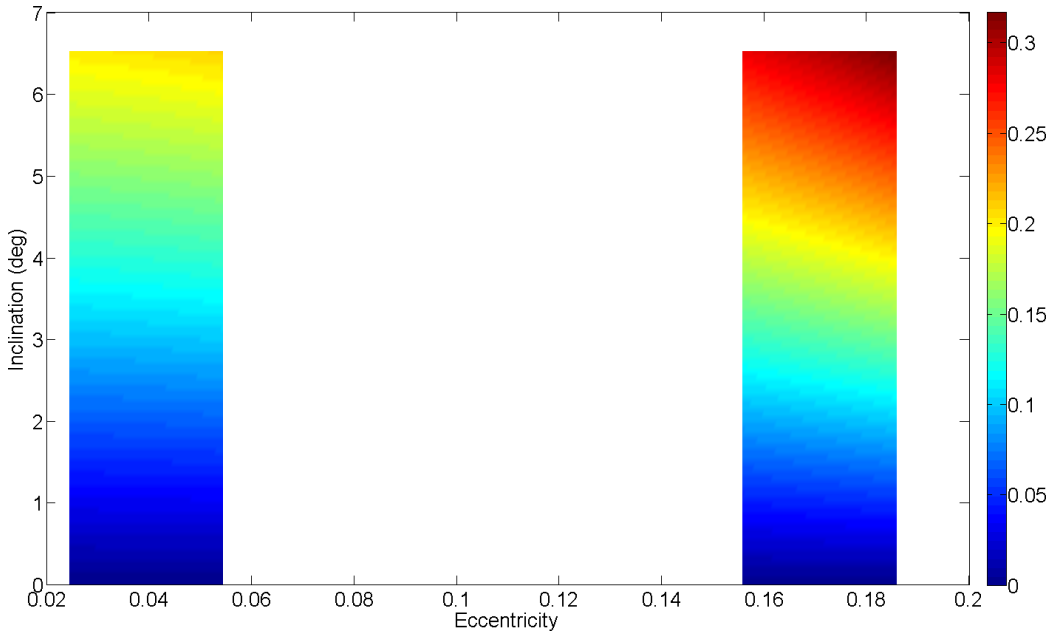

Fig. 24. Δv_Ω (m/s) for Different Eccentricities and Inclinations for $T_{\text{rep}} = 11.98$ Days (Example 3)

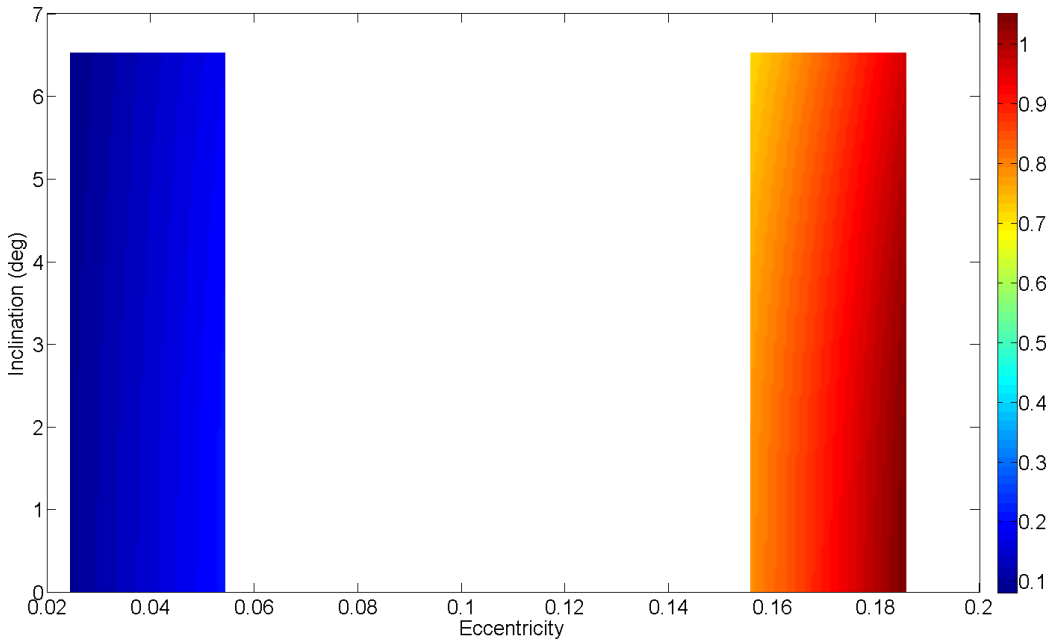

Fig. 25. Δv_ω (m/s) for Different Eccentricities and Inclinations for $T_{\text{rep}} = 11.98$ Days (Example 3)

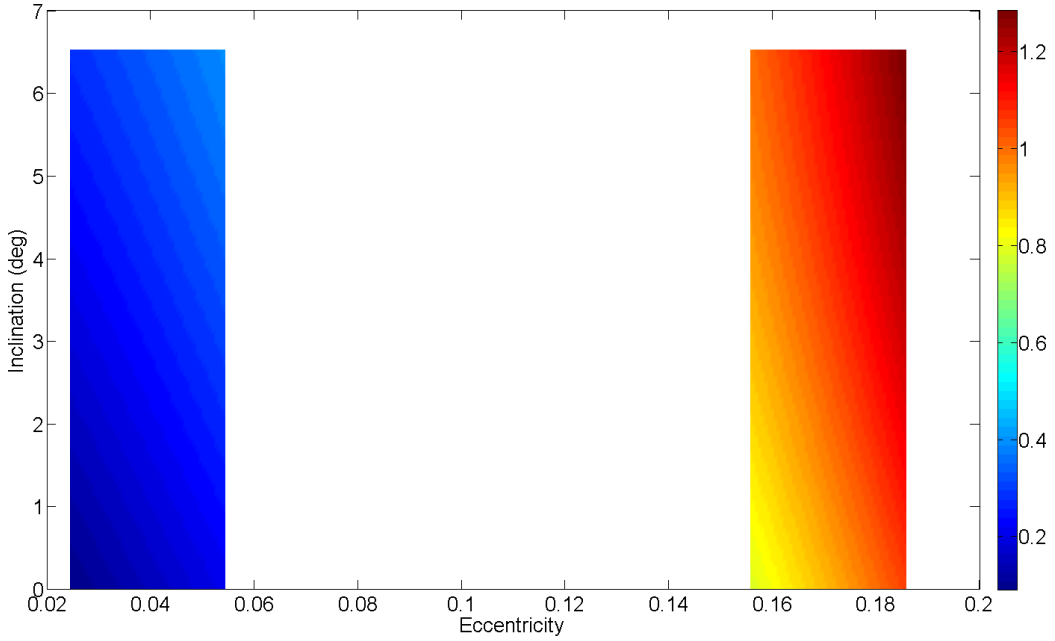

Fig. 26. Δv_{tot} (m/s) for Different Eccentricities and Inclinations for $T_{\text{rep}} = 11.98$ Days (Example 3)

CHAPTER V

CONCLUSIONS AND FUTURE WORK

The theory of Rock-Around Orbits is a useful tool for space surveillance. Its generality allows it to be applied to any target orbit regardless of its shape or orientation, and its unique orbit parameters allow it to observe an entire orbit from many different angles in a prescribed time frame. Since the RAO orbit is found with respect to the target orbit, it covers the entire target orbit passively which minimizes the Δv. Another benefit comes from using multiple spacecraft in a Flower Constellation where the spacecraft can be spaced out evenly over the RAO orbit to decrease revisit times or placed behind each other to view parts of the target orbit for longer periods of time.

There are still a few parts of the theory that need further investigation. Depending on the mission, it may be beneficial to examine the percentage of time the RAO spacecraft spends inside and outside or above and below the target orbit. Another topic of investigation is the effect of the right ascension of ascending node and the argument of perigee. For all of the analyses, Ω_r, ω_r were equal to Ω_t, ω_t. If we were to take some of the semi-major axes and eccentricity combinations that do not produce rock-around motion and intoduce a small difference in Ω_r, ω_r, or both, rock-around motion can be achieved. It is also necessary to further ivestigate the effect ω_r has on i_r and come up with a valid equation: $i_r = f(e_r, \omega_r)$. Lastly, more perturbations can be introduced such as the gravitational effects due to the Sun and Moon or atmospheric drag for Low Earth Orbits to find more accurate Δv values.

REFERENCES

[1] Mortari, D., "Flower Constellations as Rigid Objects in Space," *ACTA Futura*, Vol. 2, 2006, pp. 7-22.

[2] Mortari, D., Wilkins, M. P., and Bruccoleri, C., "The Flower Constellations," *The Journal of the Astronautical Sciences*, Vol. 52, No. 1 and 2, January–June 2004, pp. 107-127.

[3] Mortari, D. and Wilkins, M. P., "The Flower Constellation Set Theory Part I: Compatibility and Phasing," *IEEE Transactions on Aerospace and Electronic Systems*, Vol. 44, No. 3, July 2008, pp. 953-963.

[4] Wilkins, M. P. and Mortari, D., "The Flower Constellation Set Theory Part II: Secondary Paths and Equivalency," *IEEE Transactions on Aerospace and Electronic Systems*, Vol. 44, No. 3, July 2008, pp.964-976.

[5] Mortari, D., *Aerospace Technologies and Applications for Dual Use (A New World of Defense and Commercial in 21st Century Security)*, Chapter 13, pp. 105-113, River Publishers, Aalborg, Denmark, 2008.

[6] Abdelkhalik, O. O. and Mortari, D., "Two-Way Orbits," *Celestial Mechanics and Dynamic Astronomy*, Vol. 94, No. 4, April 2006, pp. 399-410.

[7] Mortari, D. and Wilkins, M. P., "Dual-Compatible Flower Constellations," *Advances in the Astronautical Sciences*, Tampa, Florida, January 22–26, 2006.

[8] "Orbital elements," Wikipedia: The Free Encyclopedia, http://en.wikipedia.org/wiki/Orbital_elements.

[9] Eberly, D., "Distance from a Point to an Ellipse in 2D," 2004, Geometric Tools LLC,
http://www.geometrictools.com/Documentation/DistancePointToEllipse2.pdf.

APPENDIX A

CONTOUR MAPS FOR DIFFERENT TARGET ECCENTRICITIES

The following figures are of the same type of plot as Figure 14 except that the eccentricity of the target orbit from Table IV varies from 0 to 0.9. Therefore, Figure 27 is for a circular target orbit with a semi-major axis of 40,000 km and Figure 32 is the same as Figure 14 because the target orbit's eccentricity is 0.5. From these figures, it can be seen how the the target orbit's eccentricity affects the percentage of time a spacecraft in a RAO Orbit is within $d_{\max}$ of the target orbit.

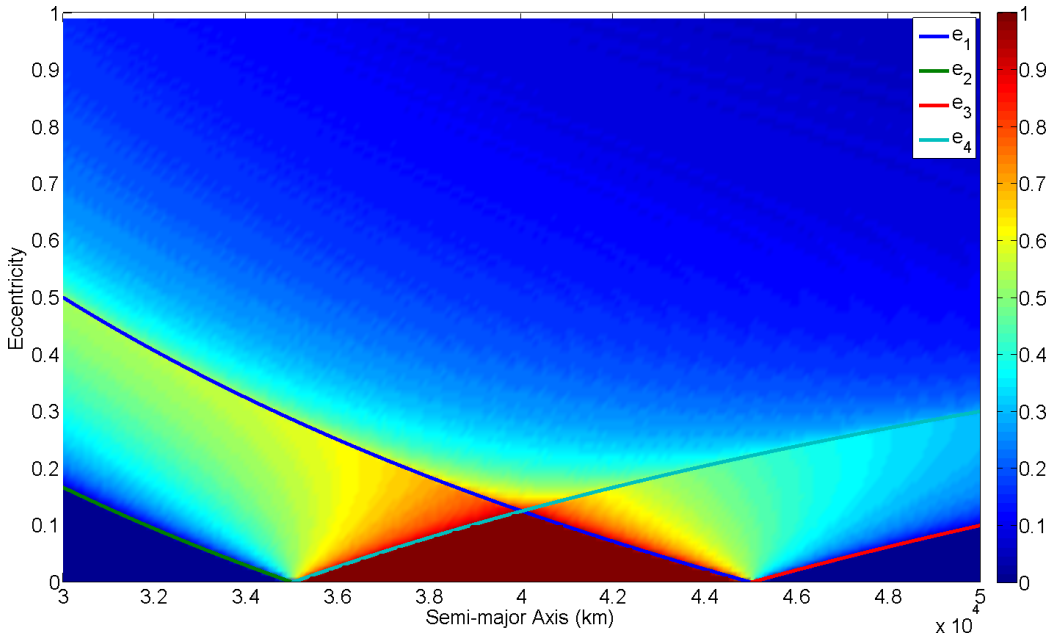

Fig. 27. Percentage of Time a Spacecraft in a RAO Orbit is within $d_{\max}$ of the Target Orbit for $e_t = 0$ (Example 2)

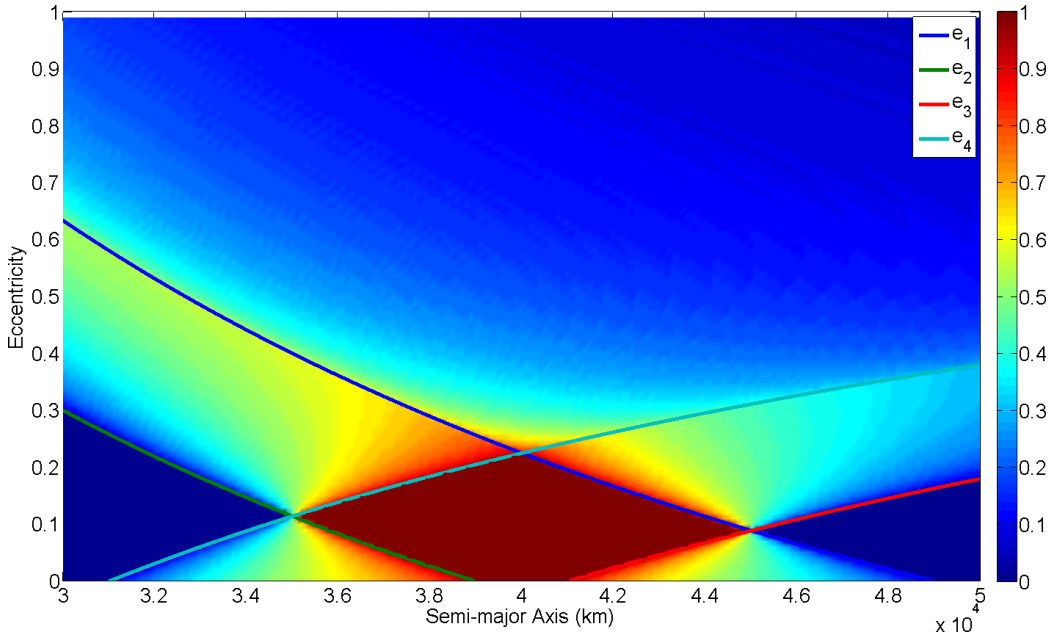

Fig. 28. Percentage of Time a Spacecraft in a RAO Orbit is within $d_{\max}$ of the Target Orbit for $e_t = 0.1$(Example 2)

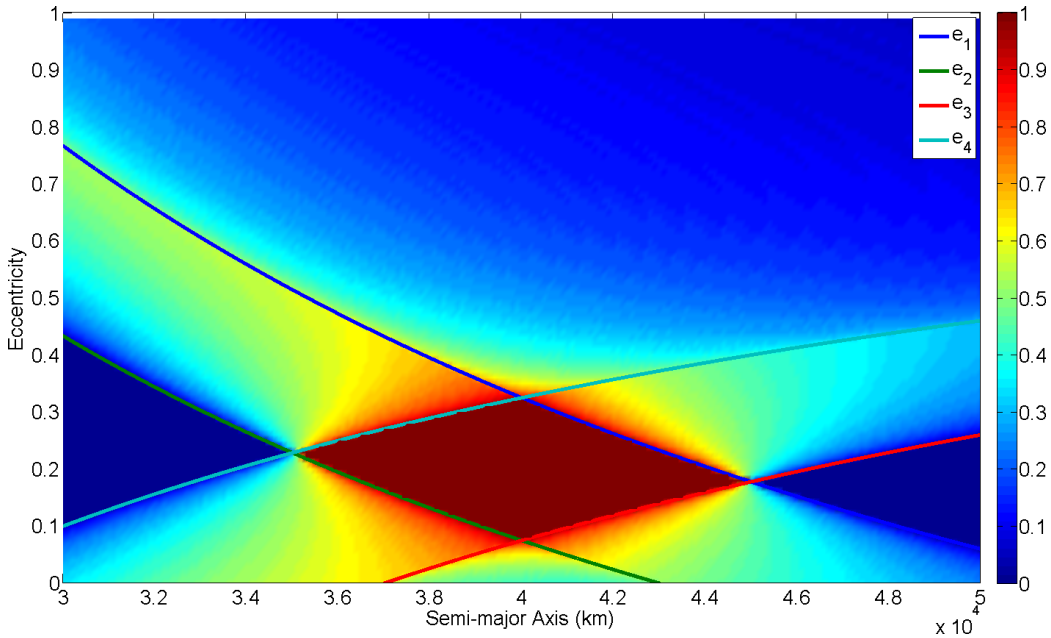

Fig. 29. Percentage of Time a Spacecraft in a RAO Orbit is within $d_{\max}$ of the Target Orbit for $e_t = 0.2$ (Example 2)

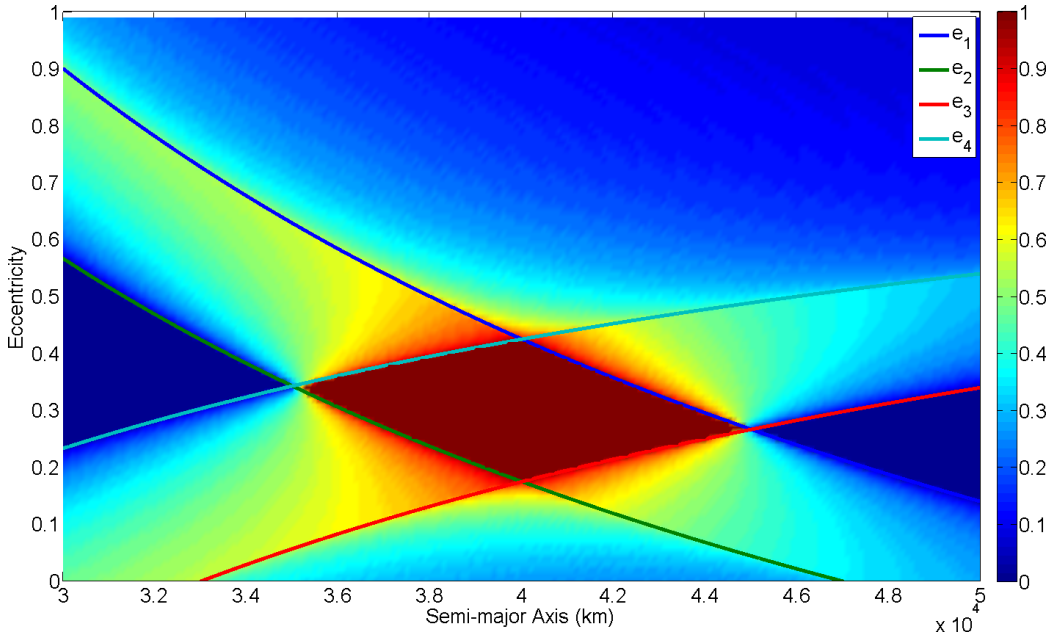

Fig. 30. Percentage of Time a Spacecraft in a RAO Orbit is within $d_{\max}$ of the Target Orbit for $e_t = 0.3$ (Example 2)

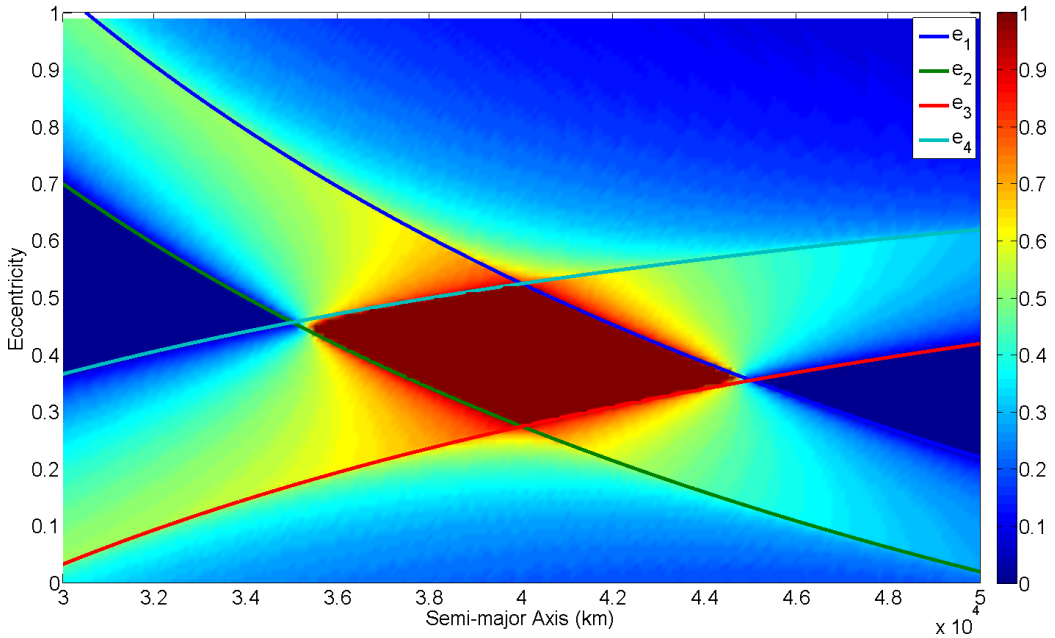

Fig. 31. Percentage of Time a Spacecraft in a RAO Orbit is within $d_{\max}$ of the Target Orbit for $e_t = 0.4$ (Example 2)

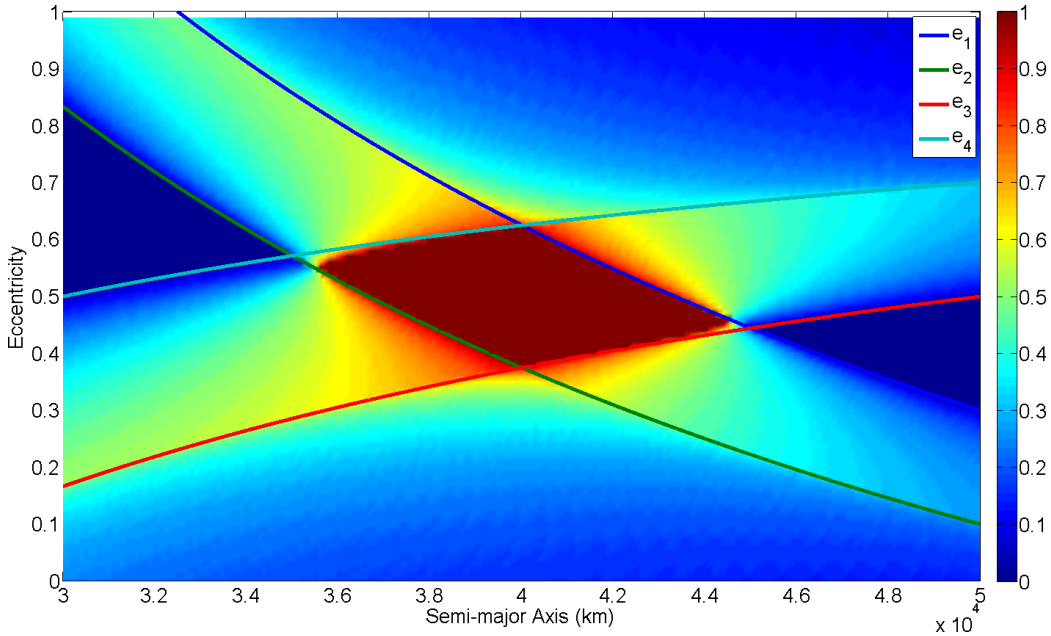

Fig. 32. Percentage of Time a Spacecraft in a RAO Orbit is within $d_{\max}$ of the Target Orbit for $e_t = 0.5$ (Example 2)

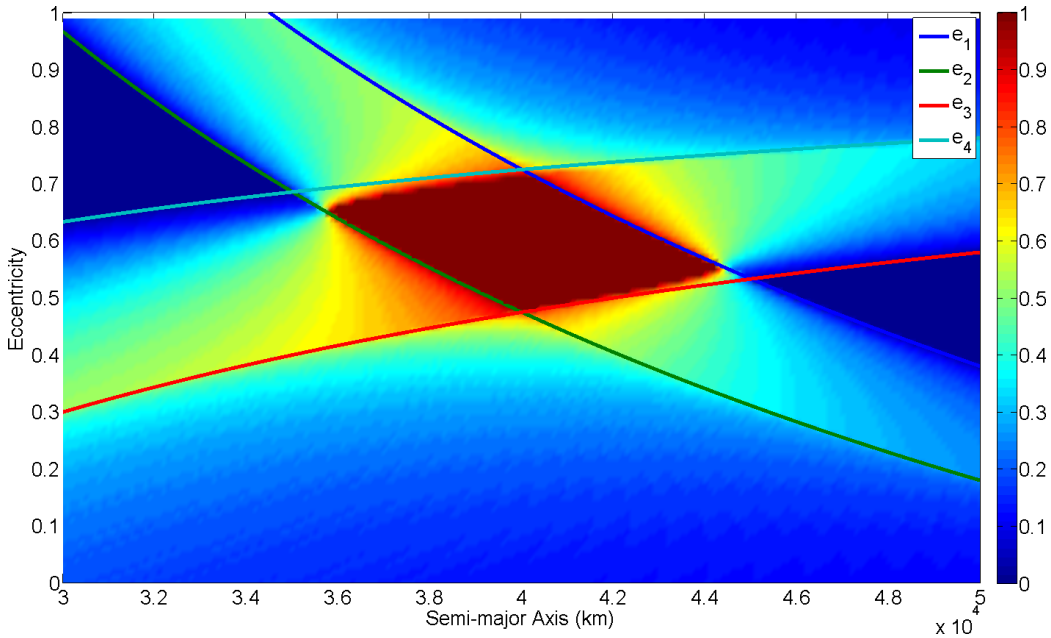

Fig. 33. Percentage of Time a Spacecraft in a RAO Orbit is within $d_{\max}$ of the Target Orbit for $e_t = 0.6$ (Example 2)

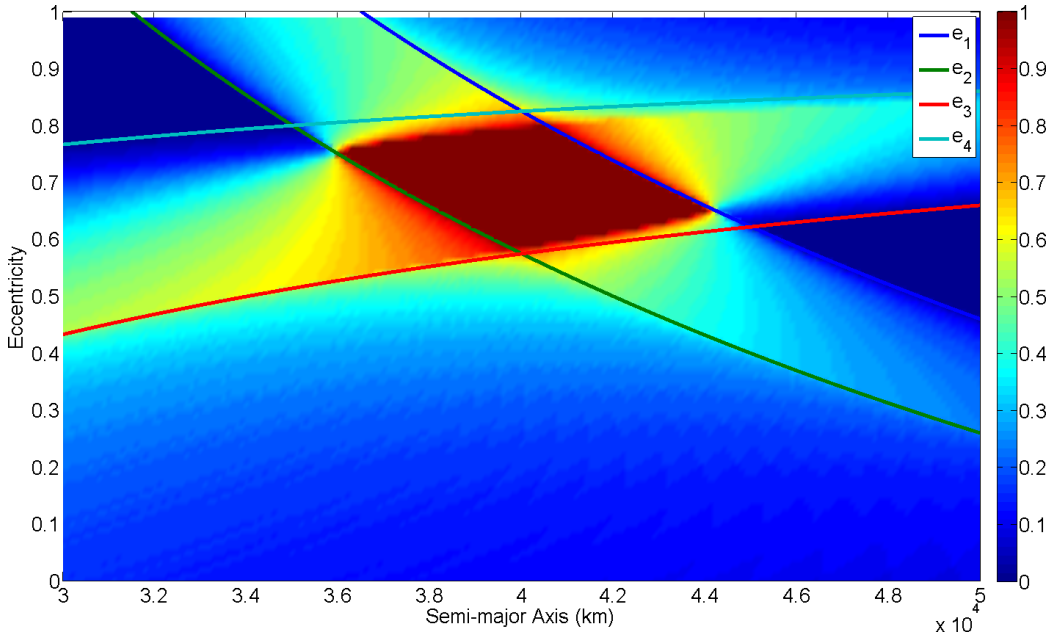

Fig. 34. Percentage of Time a Spacecraft in a RAO Orbit is within $d_{\max}$ of the Target Orbit for $e_t = 0.7$ (Example 2)

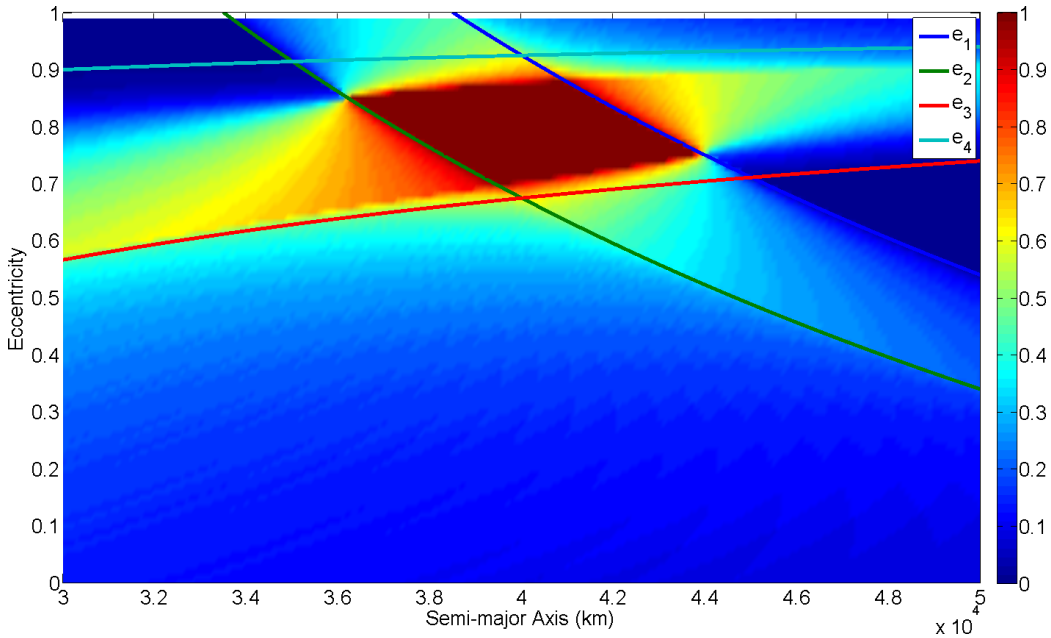

Fig. 35. Percentage of Time a Spacecraft in a RAO Orbit is within $d_{\max}$ of the Target Orbit for $e_t = 0.8$ (Example 2)

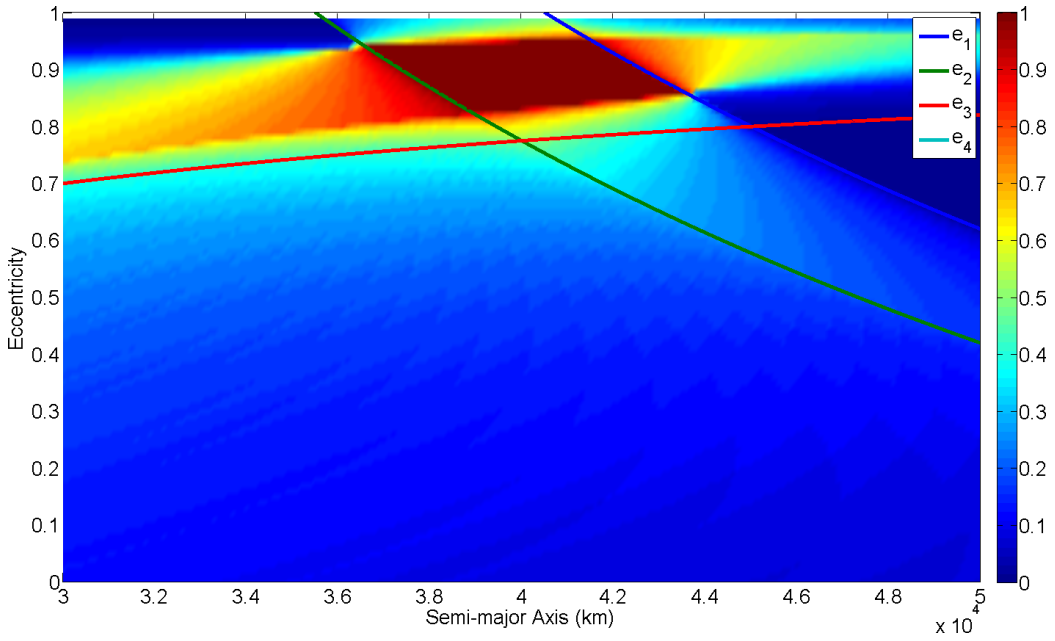

Fig. 36. Percentage of Time a Spacecraft in a RAO Orbit is within $d_{\max}$ of the Target Orbit for $e_t = 0.9$ (Example 2)

APPENDIX B

ORBIT TRAJECTORIES FOR DIFFERENT ECCENTRICITIES

The following figures are the trajectories of the TGT and RAO orbits in the inertial and rotating target orbit frames. The target orbit's parameters are defined in Table V and the RAO orbit's parameters in Table VI where the eccentricties for the four figures are eccentricity bounds from Table VI. These figures help visualize how much the eccentricity affects the shape of the RAO orbit in the rotating frame.

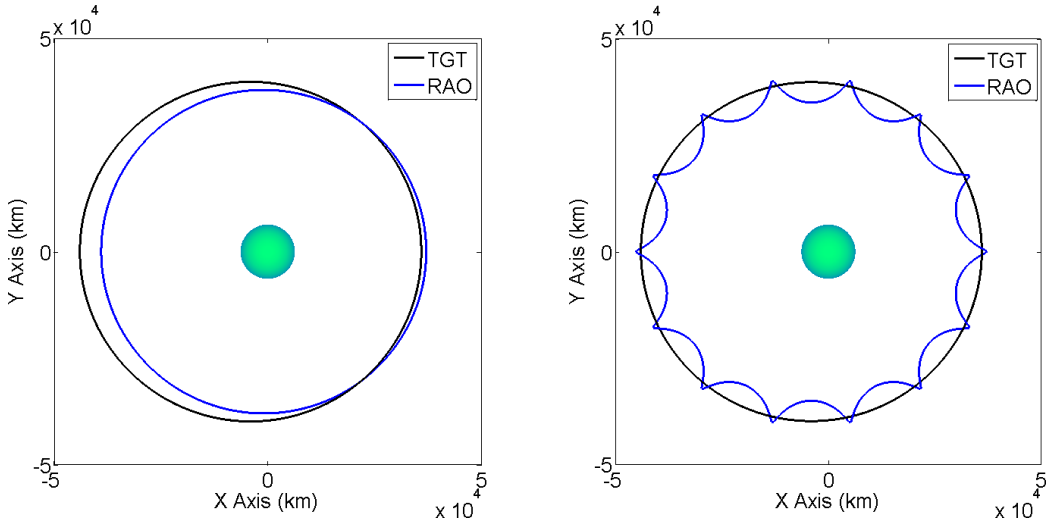

Fig. 37. TGT and RAO Orbits in the Inertial Frame and Rotating $\dot{M}_t$ Frame for $e_r = 0.0244$ (Example 3)

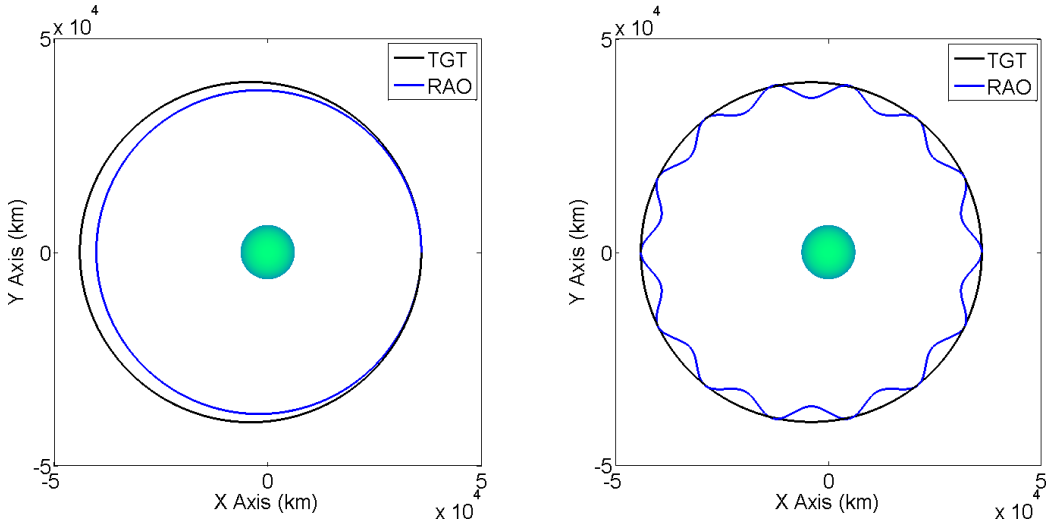

Fig. 38. TGT and RAO Orbits in the Inertial Frame and Rotating $\dot{M}_t$ Frame for $e_r = 0.0544$ (Example 3)

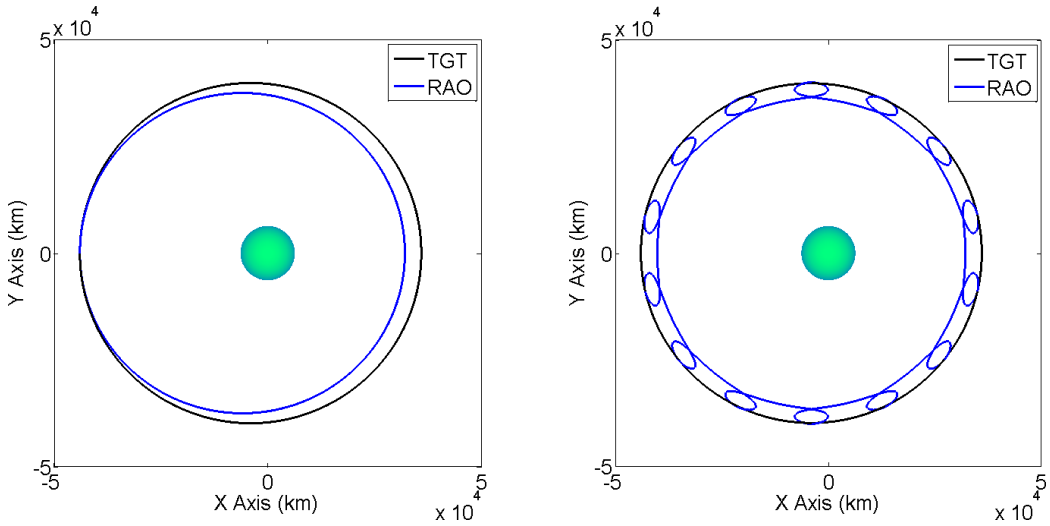

Fig. 39. TGT and RAO Orbits in the Inertial Frame and Rotating $\dot{M}_t$ Frame for $e_r = 0.1577$ (Example 3)

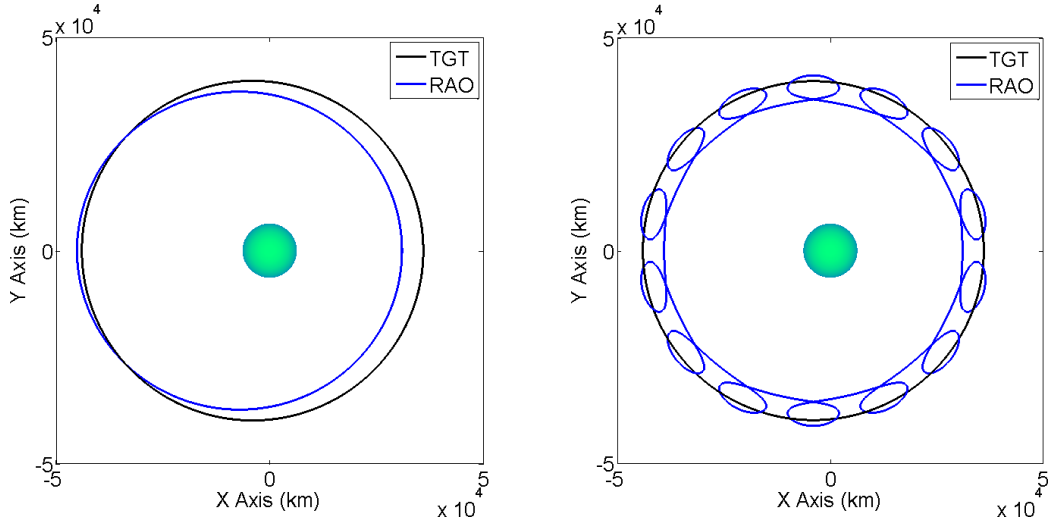

Fig. 40. TGT and RAO Orbits in the Inertial Frame and Rotating $\dot{M}_t$ Frame for $e_r = 0.1857$ (Example 3)

APPENDIX C

Δv DUE TO J_2 PERTURBATIONS

The following figures are similar to Figures 24, 25, and 26 except that $\dot{\Omega}_t$, $\dot{\omega}_t = 0$ meaning the target orbit is not drifting and therefore Δv_Ω, Δv_ω, and Δv_{tot} are the normal station-keeping requirements for the different orbits.

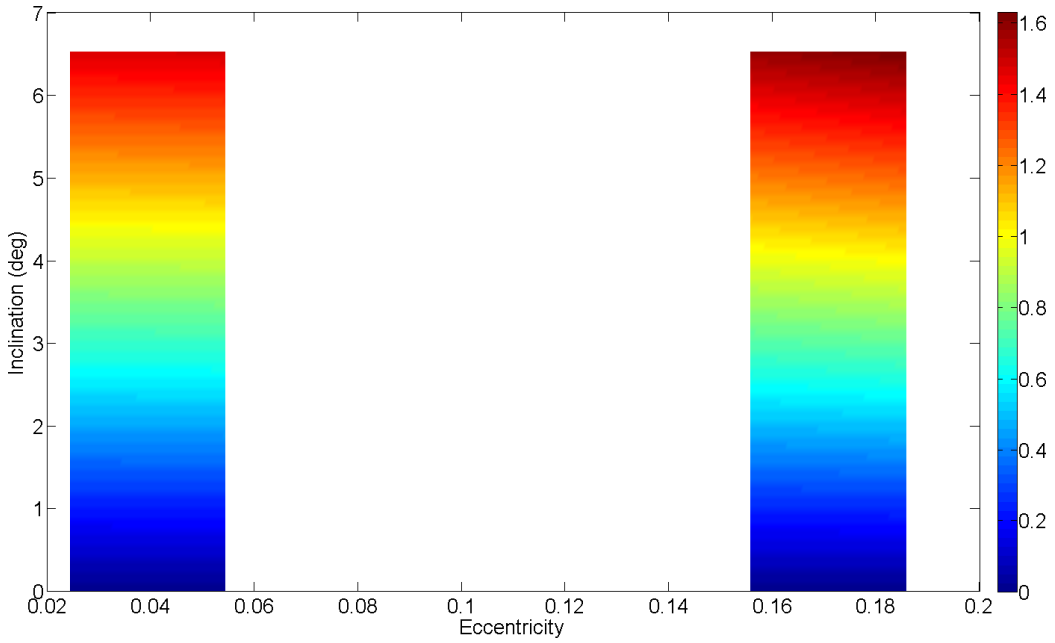

Fig. 41. Δv_Ω (km/s) for Different Eccentricities and Inclinations with $\dot{\Omega}_t = 0$ for $T_{\text{rep}} = 11.98$ Days (Example 3)

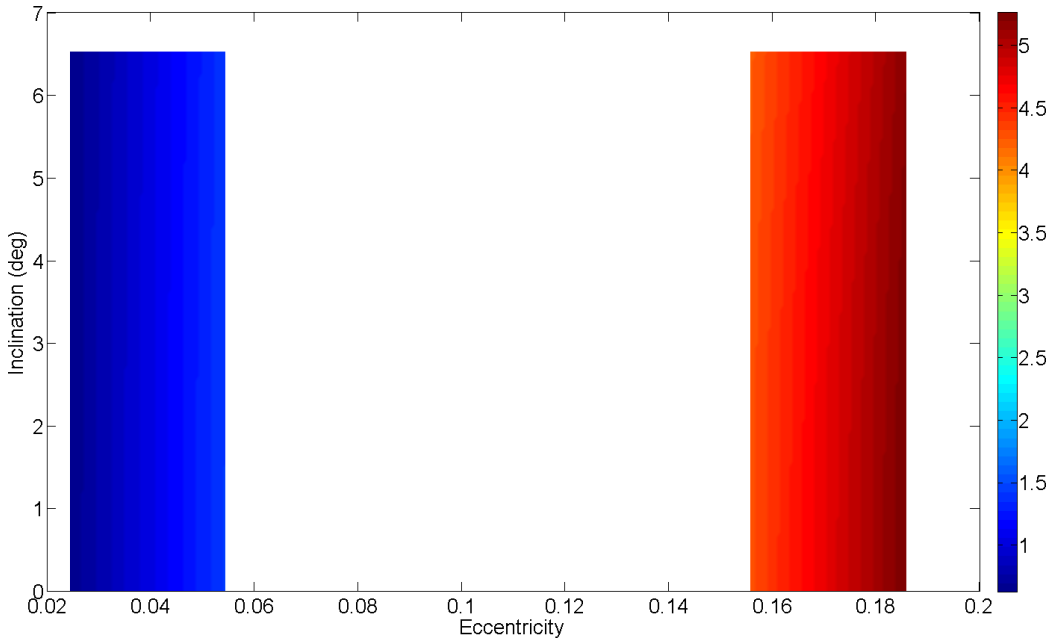

Fig. 42. Δv_ω (km/s) for Different Eccentricities and Inclinations with $\dot{\omega}_t = 0$ for $T_{\text{rep}} = 11.98$ Days (Example 3)

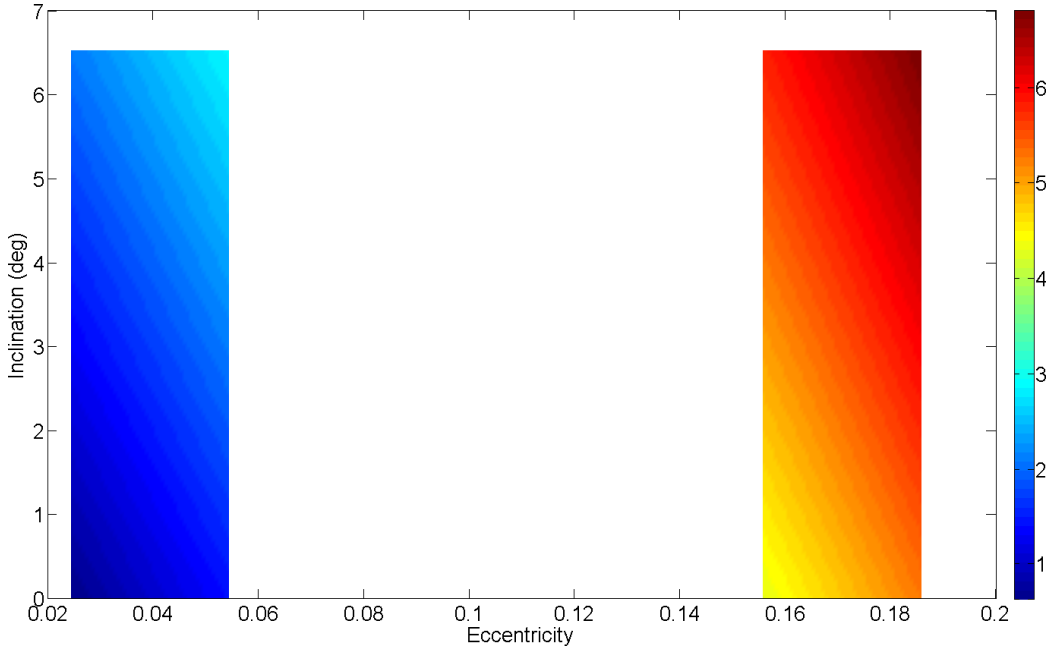

Fig. 43. Δv_{tot} (km/s) for Different Eccentricities and Inclinations with $\dot{\Omega}_t$, $\dot{\omega}_t = 0$ for $T_{\text{rep}} = 11.98$ Days (Example 3)

VITA

Scott Kenneth Bourgeois was born and raised in New Orleans, Louisiana. He received his Bachelor of Science in Aerospace Engineering from Texas A&M University in December of 2007 and his Master of Science in Aerospace Engineering from Texas A&M in December of 2009. His research interests include orbital mechanics, spacecraft dynamics and control, and space situational awareness via space-based sensors.

Scott can be reached at Texas A&M University, Department of Aerospace Engineering, 620A H.R. Bright Building, 3141 TAMU College Station, TX 77843-3141. His email address is sbourgeois@tamu.edu.